Accepted Manuscript

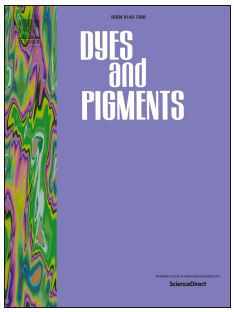

Synthesis of novel substituted methoxybenzo[2,3-*b*]carbazole derivatives via C-H functionalization. Experimental and theoretical characterization of their photophysical properties

Cinthia da Silva Lisboa, Nanci C. de Lucas, Simon J. Garden

PII: S0143-7208(16)30395-3

DOI: 10.1016/j.dyepig.2016.08.012

Reference: DYPI 5392

To appear in: *Dyes and Pigments*

Received Date: 25 May 2016

Revised Date: 1 August 2016

Accepted Date: 5 August 2016

Please cite this article as: Lisboa CdS, de Lucas NC, Garden SJ, Synthesis of novel substituted methoxybenzo[2,3-*b*]carbazole derivatives via C-H functionalization. Experimental and theoretical characterization of their photophysical properties, *Dyes and Pigments* (2016), doi: 10.1016/j.dyepig.2016.08.012.

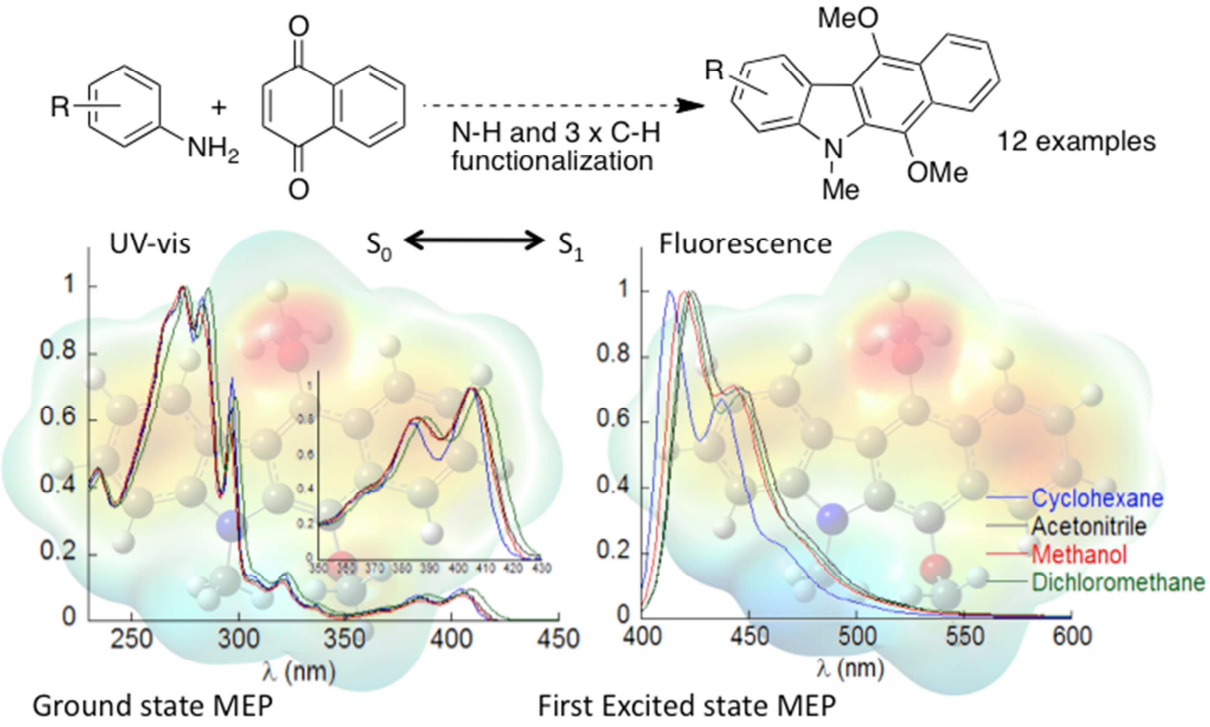

Synthesis of Novel Substituted Methoxybenzo[2,3-*b*]carbazole Derivatives via C-H Functionalization. Experimental and Theoretical Characterization of their Photophysical Properties.

Cinthia da Silva Lisboa, Nanci C. de Lucas, Simon J. Garden*

Instituto de Química, Universidade Federal do Rio de Janeiro, Cidade Universitária CT bloco A, RJ 21941-909, Brazil

* Contact information, email: garden@iq.ufrj.br

Keywords: palladium catalysis; oxidative C-H functionalization; benzo[2,3-*b*]carbazoles; UV-vis spectroscopy; time resolved fluorescence spectroscopy; density functional theory calculations.

Abstract

The novel, highly blue, fluorescent *N*-methyl-6,11-dimethoxybenzo[2,3-*b*]carbazole derivatives were prepared by oxidative coupling of anilines with naphthoquinone followed by palladium catalyzed oxidative C-H functionalization and a one pot reductive methylation reaction. The benzocarbazole fluorophores were photophysically characterized and the effects of the substituents investigated. (TD)-DFT calculations faithfully reproduced experimental photophysical properties of the benzocarbazoles and revealed how the substituents affect the photophysical properties of these compounds.

1. Introduction

Carbazole derivatives are an important class of nitrogen containing heterocyclic compounds that are widespread in nature and have been found to have useful applications. Since the isolation of carbazole in 1872 by Graebe and Glazer,[1] and later the description of the isolation and antimicrobial properties of murrayanine, a naturally occurring carbazole alkaloid from *Murraya koenigii* Spreng,[2] the intriguing structural features and promising pharmacological activities of these natural products have attracted the attention of numerous research groups. The interest in this heterocyclic system has led to the isolation of new natural compounds and an enormous effort to develop synthetic methodology for the synthesis of novel derivatives.[3] The carbazole structure is found in a wide range of compounds that possess a diverse array of pharmacological activities, including anti-tumor, antibacterial, anti-parasitic, antifungal, anti-inflammatory, and as treatments for neurological disorders.[3a, 3b, 4]

In addition to the interesting pharmacological properties of carbazole derivatives, carbazole derivatives have been increasingly attracting attention in terms of their electrical and optical properties.[5] Applications of carbazole derivatives include for example: use in organic light emitting diodes,[5m, 6] organic photorefractive materials,[7] optical sensors,[8] as an active semiconductor layer in organic field effect transistors,[9] as a fluorescent switch,[10] or as components of dye-sensitized solar cells.[6h, 11]

The present study details the synthesis and photophysical characterization of novel 6,11-dimethoxybenzo[*b*]carbazole derivatives derived from benzocarbazol-6,11-diones[12] and comparison is made with the known properties of carbazole[13]

and other derivatives of the parent heterocyclic system benzo[2,3-*b*]carbazole.[13a, 14]

2. Experimental Section

2.1 General

All reagents were purchased from Sigma-Aldrich and used as received. Spectroscopic grade solvents were used for the photophysical characterization of the benzocarbazole derivatives. ^{1}H and ^{13}C NMR spectra were recorded using either a Bruker 200 or 300 MHz spectrometer with TMS as an internal standard. Mass spectra (ESI:HRMS) were obtained with a Mass Spectrometer Q-TOF Micromass, in positive mode. Absorption spectra were recorded using a Shimatzu UV-2450 spectrophotometer. Fluorescence experiments were performed using an Edinburgh Instruments FS920 and a HITACHI F4500 spectrofluorimeter, as indicated. The fluorescence lifetime was measured using an Edinburgh Instruments FL920 CD pumped by an EPL 404.2 nm laser, also from Edinburgh Instruments. The excitation and emission wavelengths ranged from 365 to 370 nm and 420 to 465 nm, respectively.

2.2 Photophysical characterization

2.2.1 Measurement of Molar Absorption Coefficient. The molar absorption coefficient (ε) was determined from a single weighed sample dissolved in a stock solution that was subsequently diluted. The dilutions were made in such a way that the range of absorbance was from 0 to 1 (~ 10^{-5} to 10^{-6} mol/L) at the maximum wavelength and each measurement was made 5 times.

2.2.2 Fluorescence Quantum Yields (Φ_f). The fluorescence quantum yields were measured by the relative standard method,[15] in air saturated solutions, using perylene as a reference standard (Φ_f = 0.73 in cyclohexane[16]) and a FS920 Edinburgh Instruments spectrofluorimeter with a Xenon Arc Lamp (Xe900, 450 W) and a TMS300 monochromator. In this method, the Φ_f of the sample were calculated from equation 1.

$$\Phi_{f\,X} = \Phi_{f\,ST} \times (G_X/G_{ST})(\eta_X^2/\eta_{ST}^2) \qquad \text{Eq. 1}$$

The subscripts ST and X denote standard and sample, respectively; Φ_f is the fluorescence quantum yield, G the slope from the plot of integrated area of the fluorescence intensity versus absorbance and η the refractive index of the solvent (for an example see SI Figure 65). The sample and the reference were excited at the same wavelength, the same range of emission wavelengths was analyzed and both samples were maintained under the same experimental conditions.

For each Φ_f determination, the fluorescence spectra of isoabsorptive solutions (five samples in the absorbance range of 0.01 to 0.1 at the same wavelength) of the sample in an appropriate solvent (acetonitrile, dichloromethane, methanol and cyclohexane) relative to a standard solution of perylene in cyclohexane, were recorded using a 10 mm quartz cuvette.

2.2.3 Fluorescence Lifetime (τ) *Measurements.* Solutions with an absorbance of 0.1-0.5 at the absorption wavelengh (404.2 nm) were placed in quartz cuvettes. Fluorescence decay profiles of air saturated and argon-deoxygenated (15 min) solutions were recorded with the use of a fluorescence lifetime spectrometer FL920 from Edinburgh Instruments. Decays were monitored at the corresponding emission

maxima of the compounds. The FAST software, Edinburgh Instruments, allowed the fitting of the decay spectra and yielded the fluorescence lifetimes.

2.3 Theoretical calculations

The theoretical calculations were performed using Gaussian 09 rev. C.01.[17] The density functional methods B3LYP,[18] PBE0,[19] CAM-B3LYP,[20] ωB97X-D[21] were used in conjunction with Pople's double-ζ basis set augmented with diffuse functions and polarized with d orbitals.[22] Previous studies substantiate the effectiveness of this basis set for calculation of UV-vis spectra.[23]

*2.4 Synthesis and Characterization of **5**.* The methyl benzo[*b*]carbazolediol ethers **5** were prepared as shown in scheme 1. The substituents are detailed in Table 1. The first step was an oxidative coupling of naphthoquinone with anilines to give anilinonaphthoquinones (**3**), using catalytic quantities of copper acetate with acetic acid as the solvent.[24] The benzo[*b*]carbazolediones **4** were prepared by oxidative cyclization of **3** in an analogous fashion to a literature procedure.[25] The final step involved the one pot reduction and methylation using sodium dithionite and methyl iodide adapting a previously reported procedure.[26]

*2.4.1 Preparation of compounds **4***

2-Anilino-1,4-naphthoquinone **3** (0,5 mmol), $Pd(OAc)_2$ (10 mol%), $Cu(OAc)_2.H_2O$ (20 mol%), K_2CO_3 (20 mol%) and pivalic acid (2 g) were added to a round bottomed flask and closed with a septum to which an oxygen filled balloon was connected. The reaction mixture was heated at 130°C under an O_2 atmosphere for 14-20 hours. The substrate consumption was monitored by TLC and after complete

consumption the volatiles were removed under reduced pressure. The resulting crude product was taken up in a minimal volume of CH_2Cl_2 and applied to a column of chromatography silica gel. The column was eluted with CH_2Cl_2 and an EtOAc gradient. The fractions containing the product **4** were combined and the volatiles removed under reduced pressure.

*2.4.2 Preparation of compounds **5***

To the reaction flask were added: benzo[*b*]carbazolequinone **4** (0.25mmol), $Na_2S_2O_4$ (2mmol), Bu_4NBr (0.1-1mmol) and a mixture of THF/H_2O (1:1V/V, 10mL). The reaction flask was closed with a septum but allowed to pressure equalize with the atmosphere via an open syringe needle. The reaction was stirred at room temperature for about one hour or until the reaction color had faded. Subsequently, NaOH (10mmol) and an excess of CH_3I (1-2 mL) were added and the reaction was left stirring at room temperature for another hour. The crude product was isolated by partitioning the reaction between dichloromethane and water. The organic extracts were dried over Na_2SO_4, filtered and evaporated onto silica. The silica adsorbed product was applied to a short column of chromatography silica gel and the column eluted with dichloromethane. Fractions containing the product were identified by TLC, combined, and evaporated to give the isolated purified product.

*2.5 Spectroscopic structural characterization of compounds **5***

2.5.1 6,11-Dimethoxy-5-methylbenzo[*b*]carbazole **5a**: 81% yield; FT-IR (cm^{-1}; KBr): 3062, 3030, 2987, 2931, 2850, 2831, 1633, 1604, 1462, 1444, 1394, 1363, 1296, 1083, 997, 765, 744; ^1H NMR (200MHz, $CDCl_3$): δ 8.38 (3H, m); 7.48 (5H, m); 4.21 (6H, s); 4.09 (3H, s); ^{13}C NMR (50MHz, $CDCl_3$): δ 147.2; 143.6; 134.9; 132.1; 127.2;

126.9; 125.0; 123.4; 122.4; 122.3; 122.0; 121.4; 120.7; 119.3; 118.0; 107.7; 62.9; 61.2; 31.1; ESI:HRMS (m/z + H^+): calculated 292.1332; found 292.1329 ($C_{19}H_{18}NO_2^+$).

2.5.2 6,11-Dimethoxy-3,5-dimethylbenzo[*b*]carbazole **5b**: 57% yield. FT-IR (cm^{-1}, KBr):. 3074, 3062, 3000, 2929, 2850, 2831, 1633, 1604, 1461, 1442, 1429, 1396, 1359, 1311, 1295, 1211, 1193, 1176, 1149, 1128, 1103, 1081, 1051, 1020, 995, 968, 950, 906, 838, 808, 769, 736, 707. ^{1}H NMR (300MHz, $CDCl_3$): δ 8.34 (1H, d, *J* = 9.0); 8.27 (2H, m); 7.56 (1H, t, *J* = 6.0); 7.47 (1H, t, 6.0); 7.20 (1H, s); 7.15 (1H, d, *J* = 9.0); 4.19 (6H, s); 4.08 (3H, s); 2.64 (3H, s); ^{13}C NMR (75MHz, $CDCl_3$): δ 146.6; 143.9; 137.2; 134.7; 132.1; 126.8; 124.6; 124.3; 122.9; 122.2; 121.8; 120.6; 120.5; 118.8; 117.9; 108.0; 77.2; 62.8; 61.0; 30.8; 22.0; ESI:HRMS (m/z^+): calculated 305.1410; found 305.1414 ($C_{20}H_{19}NO_2^+$).

2.5.3 6,11-Dimethoxy-2,5-dimethylbenzo[*b*]carbazole **5c**: 60% yield. FT-IR (cm^{-1}, KBr):. 3064, 3023, 2987, 2933, 2856, 2832, 1737, 1633, 1616, 1583, 1490, 1463, 1444, 1407, 1390, 1361, 1338, 1294, 1241, 1230, 1218, 1189, 1166, 1157, 1145, 1108, 1081, 1051, 1006, 970, 944, 883, 848, 798, 765, 746, 701, 692. ^{1}H NMR (200MHz, $CDCl_3$): δ 8.22 (2H, m); 8.11 (1H, s); 7.33 (3H, m); 7.16 (1H, d, *J* = 8.0); 4.08 (3H, s); 4.06 (3H, s); 3.96 (3H, s); 2.50 (3H, s); ^{13}C NMR (50MHz, $CDCl_3$): δ 147.5; 142.2; 135.2; 132.8; 129.0; 128.3; 127.5; 125.2; 123.8; 122.6; 122.4; 122.4; 121.8; 120.9; 118.2; 107.7; 63.1; 61.3; 31.3; 21.5; ESI:HRMS (m/z): calculated 305.1410; found 305.1406 ($C_{20}H_{19}NO_2^+$).

2.5.4 4,6,11-Trimethoxy-5-methylbenzo[*b*]carbazole **5d**: 84% yield. FT-IR (cm^{-1}, KBr): 3066, 2990, 2953, 2931, 2832, 1629, 1585, 1456, 1360, 1308, 1254, 1082, 766, 734. ^{1}H NMR (200MHz, $CDCl_3$): δ 8.33 (2H, t, *J* = 8.0); 8.09 (1H, d, *J* = 6.0); 7.53 (3H, m); 7.25 (1H, t, *J* = 8.0); 7.07 (1H, d, *J* = 6.0); 4.49 (3H, s); 4.18 (3H, s); 4.08 (3H, s); 4.04 (3H, s); ^{13}C NMR (50MHz, $CDCl_3$): δ 147.3; 147.0; 135.8; 133.5; 127.6; 125.2; 123.9; 122.8; 122.7; 122.3; 121.1; 120.4; 118.8; 116.6; 109.5; 62.9; 61.6; 56.1; 34.6; ESI:HRMS (m/z + H^+): calculated 322.1438; found 322.1423 ($C_{20}H_{20}NO_3^+$).

2.5.5 3,6,11-Trimethoxy-5-methylbenzo[*b*]carbazole **5e**: 81% yield. FT-IR (cm^{-1}, KBr): 3061, 2997, 2926, 2849, 2833, 1605, 1460, 1359, 1296, 1231, 1080, 769. ^{1}H NMR (200MHz, $CDCl_3$): δ 8.29 (2H, m); 8.27 (1H, d, *J* = 8.0); 7.51 (2H, m); 6.92 (1H, dd, *J* = 2.0; *J* = 8.0); 6.85 (1H, d, *J* = 2.0); 4.16 (3H, s); 4.15 (3H, s); 4.06 (3H, s); 3.98 (3H, s); ^{13}C NMR (50MHz, $CDCl_3$): δ 160.3; 146.3; 145.5; 135.1; 132.7; 126.8; 124.9; 124.4; 122.8; 122.7; 122.1; 120.9; 118.2; 115.3; 107.1; 93.2; 63.2; 61.3; 55.8; 31.3; ESI:HRMS (m/z + H^+): calculated 322.1438; found 322.1428 ($C_{20}H_{20}NO_3^+$).

2.5.6 2,6,11-Trimethoxy-5-methylbenzo[*b*]carbazole **5f**: 76% yield. FT-IR (cm^{-1}, KBr): 3065, 2991, 2934, 2903, 2848, 2831, 1634, 1618, 1609, 1584, 1488, 1363, 1083, 1000, 765, 744, 459. ^{1}H NMR (200MHz, $CDCl_3$): δ 8.21 (1H, d, *J* = 8.0); 8.13 (1H, d, *J* = 8.0); 7.84 (1H, d, *J* = 2.0); 7.39 (2H, m); 7.15 (1H, d, *J* = 2.0); 7.08 (1H, dd; *J* = 2.0; *J* = 8.0); 4.06 (6H, s); 3.93 (3H, s); 3.87 (3H, s); ^{13}C NMR (50MHz, $CDCl_3$): δ154.0; 147.5; 138.9; 135.2; 133.0; 127.5; 125.3; 122.5; 122.3; 122.2; 120.9; 118.2; 115.3; 108.6; 107.7; 63.1; 61.6; 56.4; 31.4; ESI:HRMS (m/z + H^+): Calculated; 322.1438; found 322.1446 ($C_{20}H_{20}NO_3^+$).

2.5.7 1,5-Dimethyl-4,6,11-trimethoxybenzo[*b*]carbazole **5g**: 80% yield. ; FT-IR (cm^{-1}, KBr): 3067, 2991, 2933, 2832, 1360, 1291, 1259, 1087, 1062, 971, 766. ^{1}H NMR (200MHz, $CDCl_3$): δ 8,30 (2H, m). 7.49 (2H, m); 7.01 (1H, d, *J* = 8.0); 6.96 (1H, d, *J* = 8.0); 4.44 (3H, s); 4.05 (3H; s); 4.01 (3H, s); 3.98 (3H, s); 3.05 (3H, s); ^{13}C NMR (50MHz, $CDCl_3$): δ 147.2; 145.4; 136.0; 135.1; 134.9; 127.8; 127.4; 125.6; 123.7; 123.3; 123.1; 123.0; 123.0; 121.1; 119.7; 110.4; 63.6; 62.6; 56.6; 35.2; 22.8 ESI:HRMS (m/z + H^+): calculated 336.1594; found 336.1579 ($C_{21}H_{22}NO_3^+$).

2.5.8 2-Chloro-6,11-dimethoxy-5-methylbenzo[*b*]carbazole **5h**: 41% yield. FT-IR (cm^{-1}, KBr): 3311, 3066, 2991, 2934, 2833, 1636, 1604, 1482, 1456, 1361, 1339, 1297, 1083, 999, 799, 765, 698, 657. ^{1}H NMR (200MHz, $CDCl_3$): δ 8.33 (1H, d, *J* = 2.0); 7.27 (1H, m); 7.52 (4H, m); 7.29 (1H, d, *J* = 4.0); 4.17 (6H, s); 4.07 (3H, s); ^{13}C NMR (50MHz, $CDCl_3$): δ147.8; 142.3; 135.4; 132.6; 127.9; 127.1; 125.7; 124.9; 123.2; 123.0; 122.9; 122.6; 122.5; 121.0; 117.3; 108.9; 63.3; 61.7; 31.5; ESI:HRMS (m/z + H^+): calculated 326.0942; found 326.0933 ($C_{19}H_{17}ClNO_2^+$).

2.5.9 6,11-Dimethoxy-5-methyl-3-trifluoromethylbenzo[*b*]carbazole **5i**: 15% yield. FT-IR (cm^{-1}, KBr): 3068, 3035, 2993, 2939, 2850, 2835, 2721, 1641, 1614, 1481, 1462, 1444, 1367, 1328, 1292, 1168, 1103, 1083, 1060, 999, 948, 759. ^{1}H NMR (200MHz, $CDCl_3$): δ 8.46 (1H, d, *J* = 8.0); 8.33 (1H, d, *J* = 8.0); 8.26 (1H, d, *J* = 8.0); 7.53 (4H, m); 4.25 (3H, s); 4.18 (3H, s); 2.99 (3H, s); ^{13}C NMR (50MHz, $CDCl_3$): δ 148.3; 143.3; 135.5; 132.8; 129.2; 128.3; 126.0; 124.6; 123.8; 123.2; 122.8; 122.6; 121.1; 117.2; 116.3; 105.1; 63.4; 61.8; 31.5; ESI:HRMS (m/z + H^+): calculated 360.1206; found 360.1196 ($C_{20}H_{17}FNO_2^+$).

2.5.10 3-Fluoro-6,11-dimethoxy-5-methyl-benzo[*b*]carbazole **5j**: 53% yield of isomer mixture from which a sample of **5j** was separated. FT-IR (cm^{-1}, KBr): 3066, 2987, 2929, 2850, 2834, 1614, 1592, 1492, 1459, 1444, 1429, 1396, 1361, 1342, 1297, 1228, 1191, 1168, 1097, 1081, 1052, 998, 973, 958, 919, 825, 806, 765, 707. ^{1}H NMR (200MHz, $CDCl_3$): δ 8.28 (3H, m); 7.51 (2H, m); 7.02 (2H, m); 4.14 (3H, s); 4.06 (3H, s); ^{13}C NMR (50MHz, $CDCl_3$): δ [165.5; 160.6 ($^{1}J_{C-F}$ 240Hz)]; 147.0; 145.0 (J_{C-F} 10Hz); 135.3; 132.7; 127.3; 125.3; 124.5 (J_{C-F} 15Hz); 124.4; 123.0; 122.8; 122.2; 121.0; 117.9 (J_{C-F} 15Hz); 107.2 (J_{C-F} 20Hz); 95.4 (J_{C-F} 25Hz); 63.3; 61.4; ESI:HRMS (m/z): calculated 309.1160; found 309.1166 ($C_{19}H_{16}FNO_2^{+}$).

2.5.11 1-Fluoro-6,11-dimethoxy-5-methylbenzo[*b*]carbazole **5j'**: 53% yield of isomer mixture from which a sample of **5j'** was separated. FT-IR (cm^{-1}, KBr): 3066, 2989, 2929, 2852, 2834, 1616, 1494, 1463, 1444, 1361, 1322, 1295, 1241, 1147, 1083, 1052, 1008, 983, 968, 921, 867, 848, 790, 765, 736, 705, 690. ^{1}H NMR (300MHz, $CDCl_3$): δ 8.37 (1H, d, *J* = 6.0); 8.22 (1H, d, *J* = 9.0); 7.51 (3H, m); 7.15 (1H, d, *J* = 6.0); 6.98 (1H, dd, *J* = 9.0, *J* = 9.0); 4.20 (3H, s); 4.13 (3H, s); 4.05 (3H, s); ^{13}C NMR (75MHz, $CDCl_3$): δ [159.7; 156.4 ($^{1}J_{C-F}$ 248Hz)]; 147.7; 146.4(J_{C-F} 15Hz); 135.2; 132.3; 128.5(J_{C-F} 7.5Hz); 127.8; 125.8; 123.2; 123.1; 123.0; 120.8; 116.2(J_{C-F} 7.5Hz); 109.5(J_{C-F} 15Hz); 106.6 (J_{C-F} 23Hz); 106.3; 104.0; 104.0; 77.2; 63.6; 63.3; 31.8; ESI:HRMS (m/z + Na^{+}): calculated 332.1057; found 332.1062 ($C_{19}H_{17}FNO_2Na^{+}$).

2.5.12 2-Fluoro-6,11-dimethoxy-5-methylbenzo[*b*]carbazole **5k**: 79% yield. FT-IR (cm^{-1}, KBr): 2991, 2935, 2835, 1629, 1606, 1487, 1460, 1442, 1361, 1301, 1274, 1082, 997, 937, 862, 806, 767, 748. ^{1}H NMR (200MHz, $CDCl_3$): δ 8.33 (2H, m); 8.12

(1H, m); 7.53 (3H, m); 7.32 (1H, m); 4.19 (3H, s); 4.17 (3H, s); 4.08 (3H, s); ^{13}C NMR (50MHz, $CDCl_3$): δ [159.9; 155.2 ($^1J_{C-F}$ 235Hz)]; 147.7; 140.2; 135.3; 133.0; 127.8; 125.6; 122.8; 122.4; 122.3; 122.1(J_{C-F} 10Hz); 121.0; 117.8(J_{C-F} 5Hz); [114.7; 114.2 (J_{C-F} 15Hz)]; [109.8; 109.3(J_{C-F} 25Hz)]; 108.4 (J_{C-F} 5Hz); 63.1; 61.7; 31.4; ESI:HRMS (m/z + H^+): calculated 310.1238; found 310.1234 ($C_{19}H_{17}FNO_2^+$).

3. Results and Discussion

3.1 Synthesis

The previously unknown 6,11-dimethoxybenzocarbazoles were prepared through the sequence of reactions given in Scheme 1. The synthesis of the anilino-naphthoquinones (**3**) has been described by our group.[24] These compounds were obtained in good to excellent yields. The compounds **3** were then submitted to a palladium(II) catalyzed oxidative cyclization.[25, 27] The *meta*-substituted substrates **3** (R^2 = CH_3 **3b**, OCH_3 **3e**, CF_3 **3i**, and F **3j**) could result in the synthesis of two regioisomeric benzocarbazoldiones (**4**). However, the oxidative cyclization of **3e** and **3i** gave products that were found to be single regioisomers (**4e** and **4i**, respectively). On the other hand, the substrates **3b** and **3j** each gave a mixture of two regioisomeric products as determined by GC-MS analysis (**4b/b'** and **4j/j'**). In the former case only **4b** was isolated upon chromatographic purification, as **4b'** was a very minor component, and in the latter case the regioisomers, **4j/j'**, could not be separated. Reductive methylation of compounds **4** was performed in a one pot procedure.[26] There are a very limited number of examples of reduction of compounds **4** in the literature to give benzo[2,3-*b*]carbazole-6,11-diols. The use of zinc in acetic anhydride results in the obtention of the benzo[*b*]carbazole-6,11-diol acetate esters,[28] whilst reduction of **4** with zinc in AcOH[29] or $NaBH_4$ in MeOH[10] gives

the air unstable benzo[2,3-*b*]carbazole-6,11-diol derivatives which are rapidly oxidized back to **4**. Therefore the one pot reductive methylation of compounds **4** allowed the synthesis and facile isolation of the novel, highly blue, fluorescent 6,11-dimethoxybenzo[2,3-*b*]carbazole derivatives (**5**). The reductive methylation of the regioisomeric mixture **4j/j'** allowed the separation of the regioisomeric products **5j** and **5j'**. The new compounds **5** were structurally characterized by ^{1}H and ^{13}C NMR, FT-IR spectroscopy and high resolution mass spectrometry.

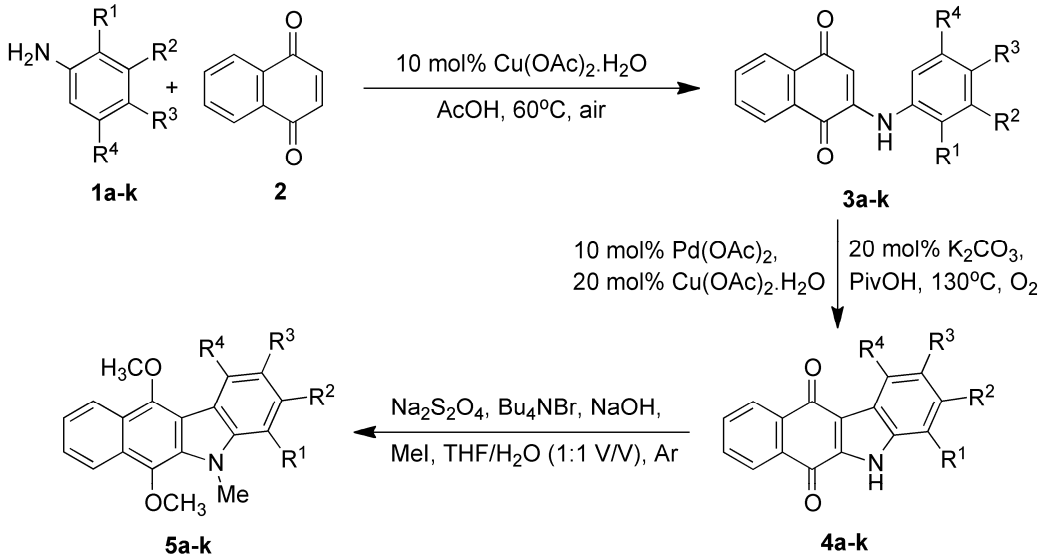

Scheme 1: Preparation of methoxybenzocarbazole derivatives (See Table 1 for substituent details).

Table 1: Substituent details for derivatives (Deriv.) of compounds **1**, **3**, **4**, and **5**.(#)

Deriv.	R^1	R^2	R^3	R^4	Deriv.	R^1	R^2	R^3	R^4
a	H	H	H	H	**f**	H	H	OMe	H
b	H	Me	H	H	**g**	OMe	H	H	Me
b'	H	H	H	Me	**h**	H	H	Cl	H
c	H	H	Me	H	**i**	H	CF_3	H	H

d	OMe	H	H	H	**j**	H	F	H	H
e	H	OMe	H	H	**j'**	H	H	H	F
e'	H	H	H	OMe	**k**	H	H	F	H

(#) For compounds **1** and **3**, **b** = **b'**, **e** = **e'**, **j** = **j'**. Compounds **4** (**b**,**b'**) and (**j**,**j'**) were obtained as mixtures of two regioisomers resulting from the oxidative cyclization of **3b** and **3j** respectively. The purification of **4b,b'** resulted in the isolation of only **4b** (the principal regioisomer of the mixture). The regioisomers **4j/j'** could not be separated and the mixture was used directly in the reductive methylation reaction. The regioisomers **5j,j'** were separated and individually characterized. In principal, the oxidative cyclization of **3e** could give rise to a regioisomeric mixture **4** (**e**,**e'**). However, the product **4e** was obtained as a single regioisomer and this was transformed into **5e**. Compound **5e'** was modeled in the theoretical study but has not been synthesized. Similarly **3i** could have given a mixture of two regioisomers, but a single regioisomer corresponding to **4i** was obtained which was subsequently transformed into **5i**.

3.2 UV-vis absorption spectroscopy

The UV-vis absorption and emission spectra of compounds **5** employed in this study were recorded in dilute solution using four solvents with different polarities: cyclohexane (Cyh), dichloromethane (DCM), acetonitrile (ACN) and methanol (MeOH) at room temperature.

The absorption spectra of compounds **5** show strong absorption bands at short wavelengths (270 - 300 nm), a weak band at slightly longer wavelengths (300 - 330 nm), and a weak band that extends into the visible region (350 - 430 nm). Figure 1 shows the absorption spectra for **5a** in four solvents of different polarities. The longest wavelength absorption band exhibits vibronic structure. A discrete bathochromic effect (0-2 nm) was observed when the solvent was changed from cyclohexane to acetonitrile (**5a**, figure 1). Although, in general, the UV-vis spectra obtained in CH_2Cl_2 revealed a marginally larger red shift relative to cyclohexane (3-4

nm, Table 2, see SI tables 2-13). Table 2 details values of λ_{max} and ε for the most intense and the lowest energy absorption bands for compounds **5** in cyclohexane as well as λ_{max} for the S_0-S_1 transition in the other solvents. Bonesi *et al*[13b] have observed a small bathochromic shift of the absorbance spectra with increasing solvent polarity for carbazole derivatives. Such a behavior is consistent with the $\pi \rightarrow \pi^*$ nature of the electronic transition associated with the first excited state. In comparison to the absorption spectrum of the parent benzo[2,3-*b*]carbazole (**6**), the spectra of **5** reveal a bathochromic shift for the longest wavelength band (aprox. 30 nm) and a considerable reduction in intensity of the intermediate band.[13a]

The absence of a significant solvatochromic effect is not unusual for polyaromatic hydrocarbons of intermediate polarity (possessing few heteroatoms within a structure that is predominantely hydrocarbon).[13b, 15b] That both apolar and polar solvents result in very similar absorption spectra must reflect differing extents of interaction (electrostatic, hydrogen bonding and or other permanent dipole-dipole interactions, as well as dispersion forces) of the solvent with the HOMO and LUMO orbitals, where the net effects with respect to the HOMO-LUMO gap result in a similar difference in energy for extremes of solvent polarity. In this context it is perhaps therefore not surprising that a solvent of intermediate polarity could therefore result in a larger bathochromic shift of the $\pi \rightarrow \pi^*$ excitation in comparison to a more (a)polar solvent.

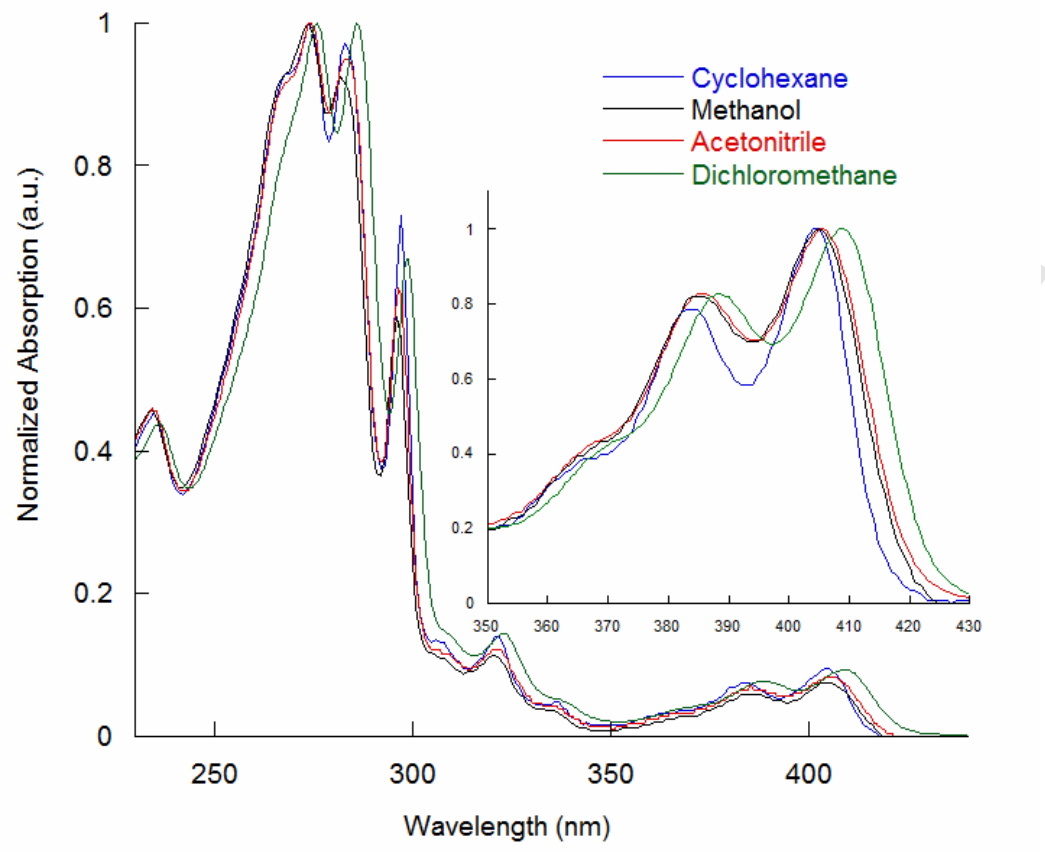

Figure 1: Normalized absorption spectra for **5a** in DCM, ACN, Cyh, and MeOH. Concentration variation from 10^{-5} to 10^{-6} mol/L and around 10^{-4} mol/L at expansion.

The data in Table 2 reveals how both the nature (Figure 2, part A - variation of the substituent R^3, part B - variation of the substituent R^2) and the position (Figure 3, fixed the nature of the substituent and varied its position) of substituents have an effect on the absorption spectra. Variation of the substituent R^3 (Figure 2A) resulted in a bathochromic shift of λ_{max} for **5c** (Me 6 nm), **5f** (OMe 16 nm), **5h** (Cl 9 nm), **5k** (F 11 nm) for the first excited state relative to the unsubstituted **5a**. In contrast, variation of R^2 (Figure 2B) resulted in a hypsochromic shift for **5b** (Me 3 nm), **5e** (OMe 14 nm), and **5j** (F 10 nm) whilst a bathochromic shift was observed for **5i** (CF_3 11 nm). The introduction of a MeO group at position R^1 gave bathochromic shifts for

5d (4 nm) and **5g** (R^4=Me, 12 nm) whilst a F substituent at R^4 gave a small hypsochromic shift (**5l** 2 nm). In a general manner, substituents with positive mesomeric or sigma electron donating effects at positions R^1 and R^3 result in a bathochromic shift whilst these same substituents at position R^2 resulted in a hypsochromic shift, with the exception of **5g**, whilst the strongly electron withdrawing substituent of **5i** (R^2 = CF_3) has the opposite effect.

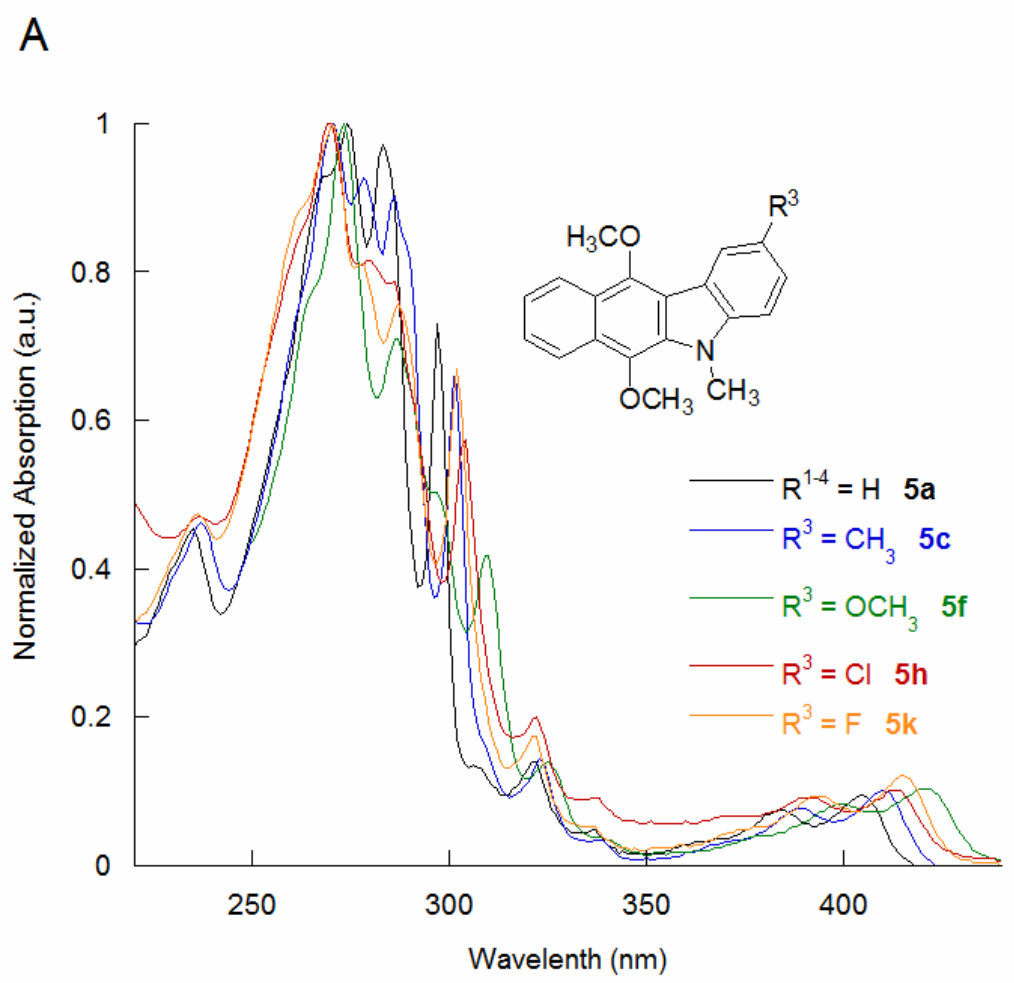

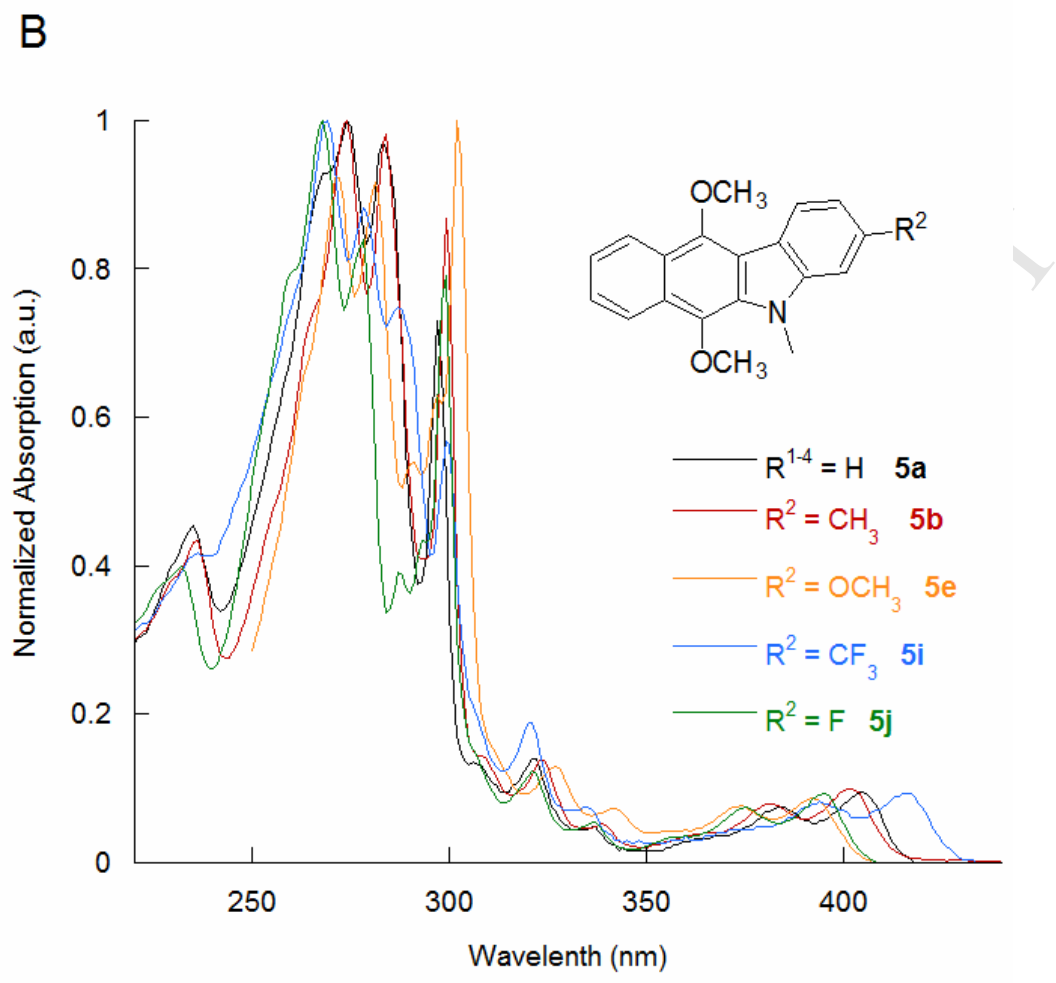

Figure 2: A) Normalized absorption spectra of **5a** and compounds **5** with a substituent at the R^3 position in cyclohexane. B) Normalized absorption spectra of **5a** and compounds **5** with a substituent at the R^2 position in cyclohexane. Concentration variation from 10^{-5} to 10^{-6} mol/L.

Table 2: Photophysical absorption and emission parameters of **5**.

Comp. (Sub.)	λ_{max} Abs (nm, Cyh)[a] *(ε 10^4.L.mol^{-1}cm^{-1})*[b]	S_0-S_1 λ_{max} Abs (nm)[a]	λ_{max} Em (nm), (Stokes shift, nm)[a,c]
5a	235, 274 *(5.42)*, 283, 297, 321, 384, 405 *(0.55)*	409 (DCM) 406 (ACN); 405 (MeOH)	413 (8 Cyh), 422 (13 DCM) 423 (17 ACN), 420 (15 MeOH)
5b	236, 274 *(2.52)*, 284, 299, 324, 339, 381, 402 *(0.26)*	405 (DCM) 404 (ACN); 401 (MeOH)	411 (9 Cyh), 419 (14 DCM) 422 (18 ACN), 418 (17 MeOH)
5c	237, 270 *(8.01)*, 301, 323, 389, 410 *(0.86)*	414 (DCM) 412 (ACN); 410 (MeOH)	421 (11 Cyh), 428 (14 DCM) 431 (19 ACN), 426 (16 MeOH)
5d	282 *(18.6)*, 322, 388, 409 *(1.03)*	412 (DCM) 409 (ACN); 407 (MeOH)	418 (9 Cyh), 431 (19 DCM) 433 (24 ACN), 429 (22 MeOH)
5e	272, 281, 302 *(6.21)*, 327, 342, 374, 392 *(0.60)*	396 (DCM) 393 (ACN); 392 (MeOH)	402 (11 Cyh)[d], 411 (15 DCM) 413 (20 ACN), 409 (17 MeOH)
5f	273 *(4.49)*, 287, 309, 325, 399, 421 *(0.48)*	425 (DCM) 422 (ACN); 421 (MeOH)	431 (10 Cyh), 443 (18 DCM) 445 (23 ACN), 441 (20 MeOH)
5g	286 *(7.72)*, 308, 324, 396, 417 *(0.42)*	418 (DCM) 416 (ACN); 414 (MeOH)	427 (10 Cyh), 443 (25 DCM) 445 (29 ACN), 440 (26 MeOH)
5h	236, 269 *(4.23)*, 304, 322, 337, 391, 413 *(0.43)*	417 (DCM) 415 (ACN); 414 (MeOH)	421 (8 Cyh), 431 (14 DCM) 432 (17 ACN), 428 (14 MeOH)
5i	269 *(6.56)*, 278, 299, 321, 335, 394, 416 *(0.64)*	419 (DCM) 417 (ACN); 416 (MeOH)	426 (10 Cyh), 437 (18 DCM) 440 (23 ACN), 437 (21 MeOH)
5j	232, 268 *(4.72)*, 278, 299, 321, 337, 375, 395 *(0.42)*	398 (DCM) 398 (ACN); 396 (MeOH)	404 (9 CH), 411 (13 DCM) 413 (15 ACN), 410 (14 MeOH)
5j'	275 *(17.3)*, 305, 319, 381, 403 *(1.23)*	406 (DCM) 405 (ACN); 404 (MeOH)	411 (8 Cyh), 418 (12 DCM) 421 (16 ACN), 417 (13 MeOH)
5k	236, 270 *(5.85)*, 287, 302, 321, 394, 415 *(0.72)*	419 (DCM) 417 (ACN); 416 (MeOH)	425 (10 Cyh), 434 (15 DCM) 435 (18 ACN), 431 (15 MeOH)

[a] Cyclohexane (Cyh), dichloromethane (DCM), acetonitrile (ACN) or methanol (MeOH) as solvent.

[b] Molar extinction coefficients of the most intense band and the lowest energy band, respectively, in cyclohexane.

[c] Excitation at 370 nm and emission range from 390-600 nm;

[d] Excitation at 365 nm and emission range from 380-600 nm.

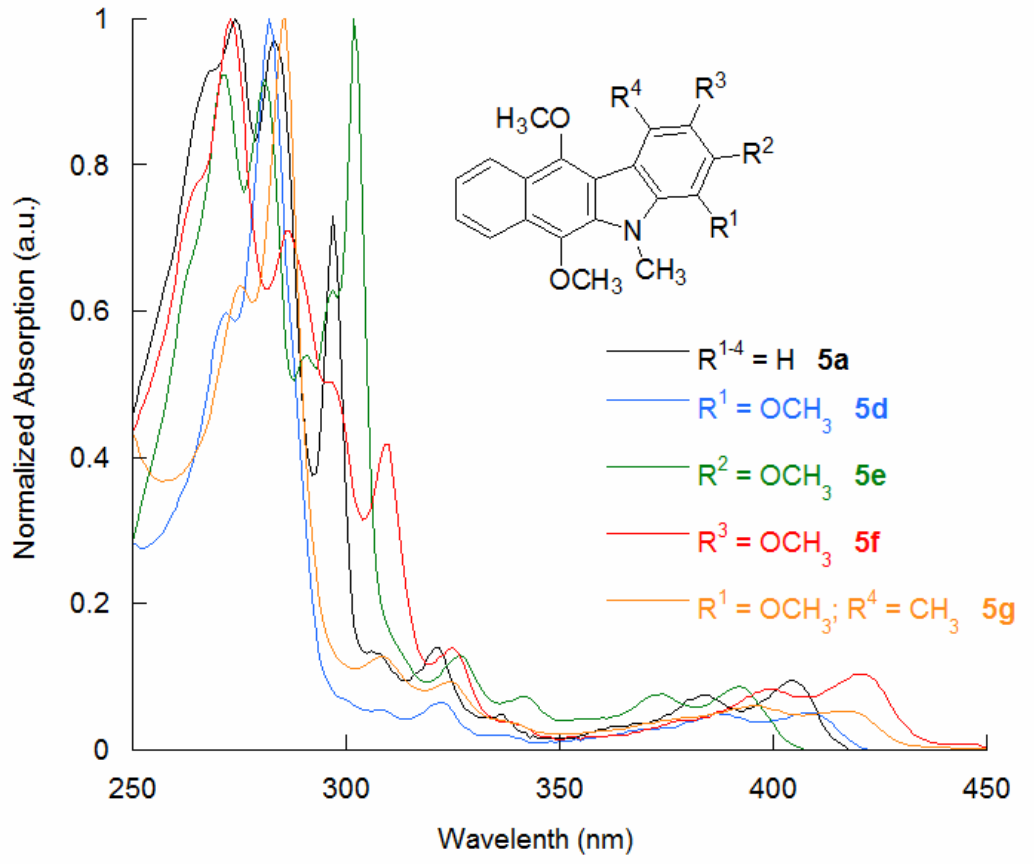

Figure 3: Normalized absorption spectra of **5a** and compounds **5** substituted with methoxy groups in cyclohexane. Concentration variation from 10^{-5} to 10^{-6} mol/L.

The large bathochromic shift of the lowest excited state of benzo[2,3-*b*]carbazole (**6**) relative to the heteroatom free benzo[2,3-*b*]fluorene has been attributed to the facile displacement of electron density from nitrogen to the naphthyl system on excitation, thus resulting in an excited state structure for which an extended

quinoid type canonical form was proposed as an important structural contribution.[13a] In principal, the compounds of the current study could present somewhat similar excited state structures (Figure 4). Using this model allows for an interpretation of how electron donating substituents R^1 (*ortho* to nitrogen) and R^3 (*para* to nitrogen) of the phenylene ring system can contribute to stabilize, and hence red shift, S_1 relative to the substituent free **5a**. The hypsochromic shift when electron donating substituents are *meta* to the nitrogen (R^2 and/or R^4) is better rationalized through consideration of the resonance model (**7**). At the same time model **7** may rationalize the large bathochromic shift for strongly electron withdrawing CF_3 (**5i**) at position R^2.

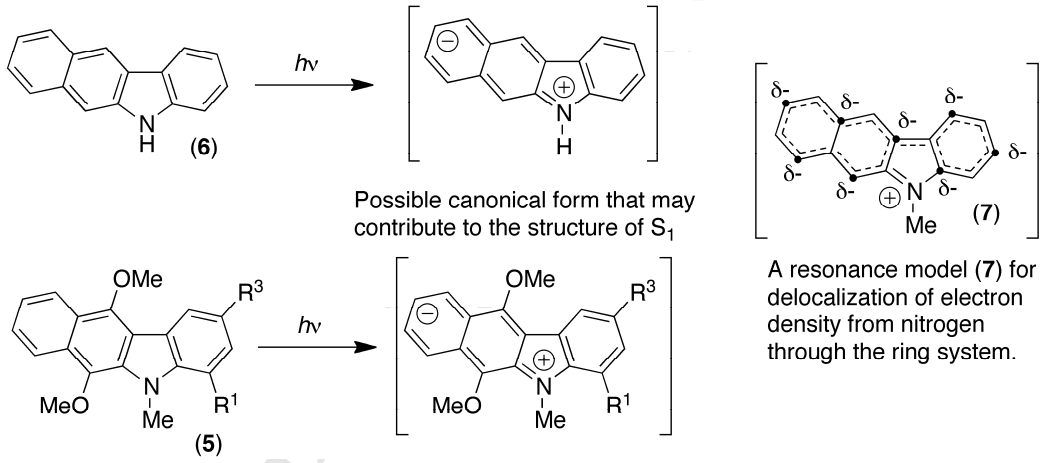

Figure 4: Resonance structure representation of a potential extended quinoid type canonical form contribution to the structure of the S_1 excited state of **5** and **6**, and a resonance model representation (**7**) of conjugated electron density delocalization.

3.3 Fluorescence spectroscopy

Figure 5 shows normalized absorption, excitation and emission spectra for **5a** in cyclohexane. The excitation and emission spectra display excellent mirror symmetry with only a small Stokes shift separating the absorption and emission

maxima. Additionally, the excitation spectrum reveals that some of the higher excited states can contribute to emission through internal conversion to the $^1S_1$ state. The fluorescence spectra of compounds **5** occur in the range of 400-500 nm and reveal vibrational structure (see also SI Figures of normalized emission spectra of **5** in the SI). Figure 6 shows the normalized emission spectra for **5a** in four solvents of different polarities (λ_{max}Em: Cyh 413nm, MeOH 420nm, DCM 422nm, ACN 423nm). A minor red shift of the emission spectra in differing solvents relative to emission in cyclohexane is observed and it is notable that emission in the protic solvent MeOH is blue shifted relative to the less polar CH_2Cl_2 or similarly polar ACN. The greater stability of the relaxed excited state in the polar solvents is reflected by the larger Stokes shift (Table 2) for emission in the polar solvents (Cyh 8 nm, MeOH 15 nm, CH_2Cl_2 13 nm, ACN 17 nm) and longer fluorescence lifetimes (Table 3, τ).[15b] The observations are consistent with the view that the excited state has a slightly larger dipole moment than the ground state.

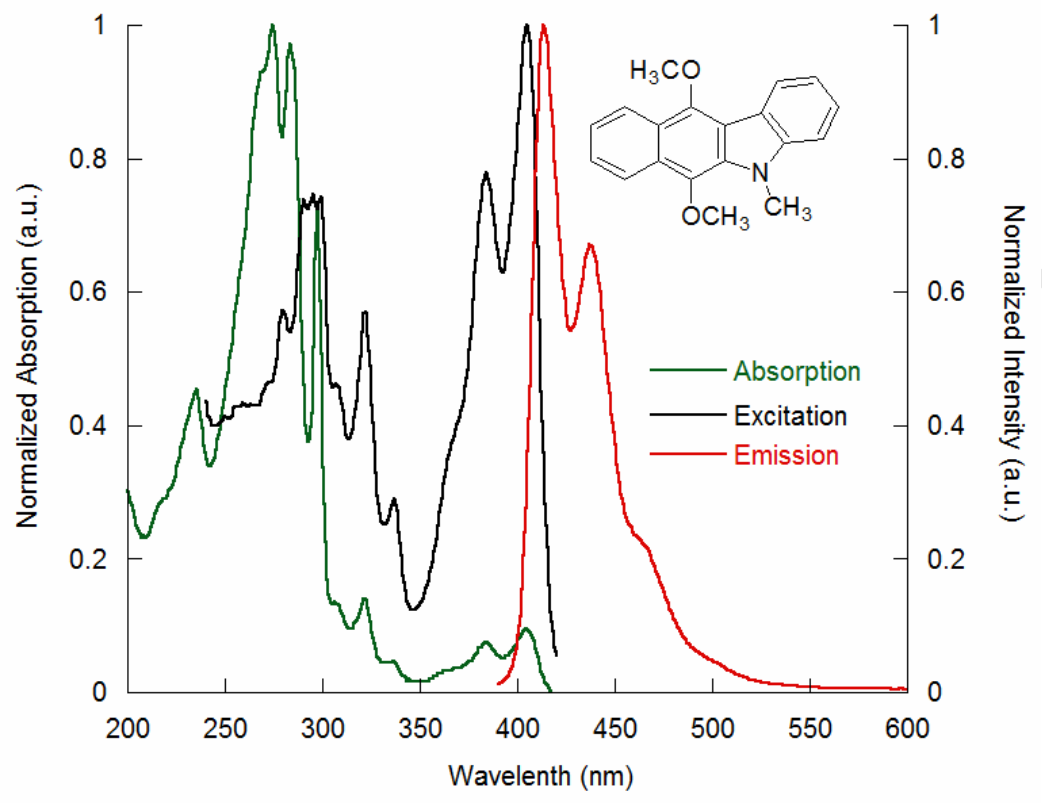

Figure 5: Normalized absorption, excitation and emission spectra of **5a** in cyclohexane.

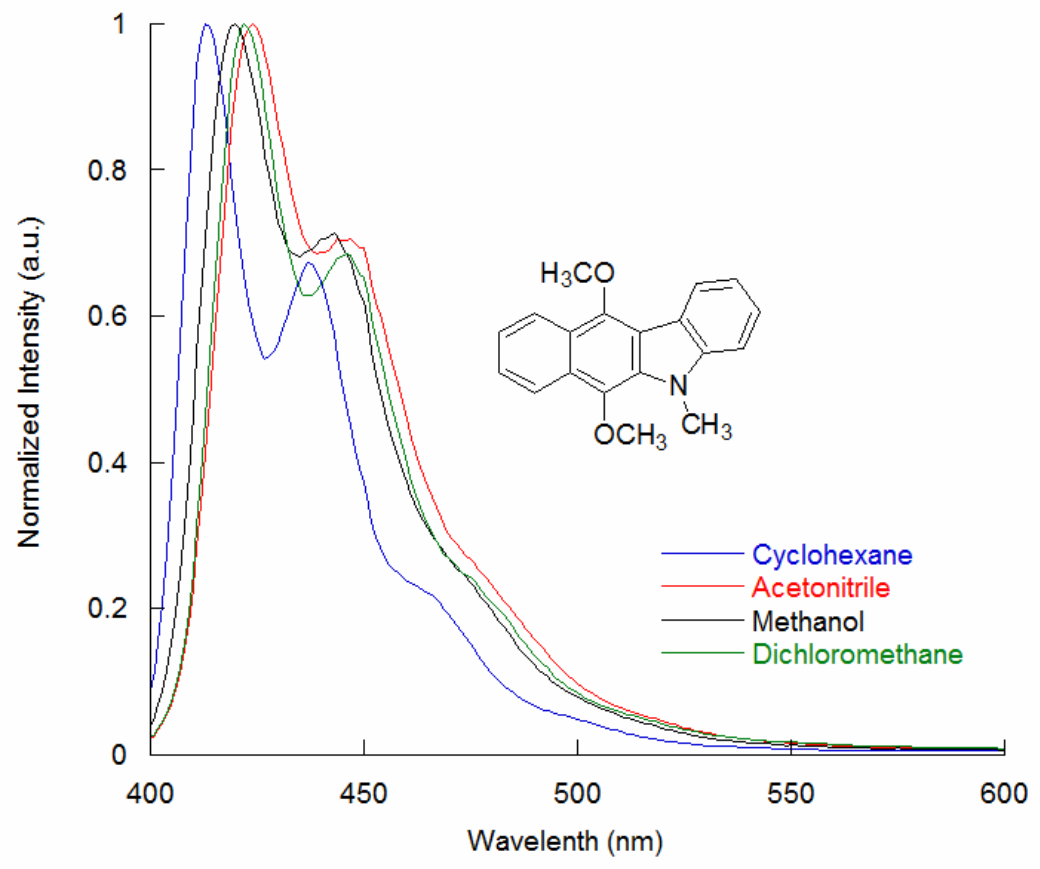

Figure 6: Normalized emission spectra for **5a**: cyclohexane, methanol, dichloromethane, acetonitrile (λ_{exc} = 370 nm).

Figure 7 reveals the effect of the variation of the nature of the substituent at a fixed position. Figure 7A compares the emission spectra, recorded in cyclohexane, of **5a** with the spectra recorded for derivatives with substituents at the R^3 position (methyl **5c,** methoxy **5f,** chlorine **5h** and fluorine **5k**) and Figure 7B compares the emission spectra for compounds **5** with a substituent at the R^2 position (methyl **5b**, methoxy **5e**, trifluoromethyl **5i** and fluorine **5j**) with **5a**. Figure 8 compares the emission spectra of **5a** with the methoxy substituted derivatives **5d-g** where the position of the substituent (MeO group) is varied.

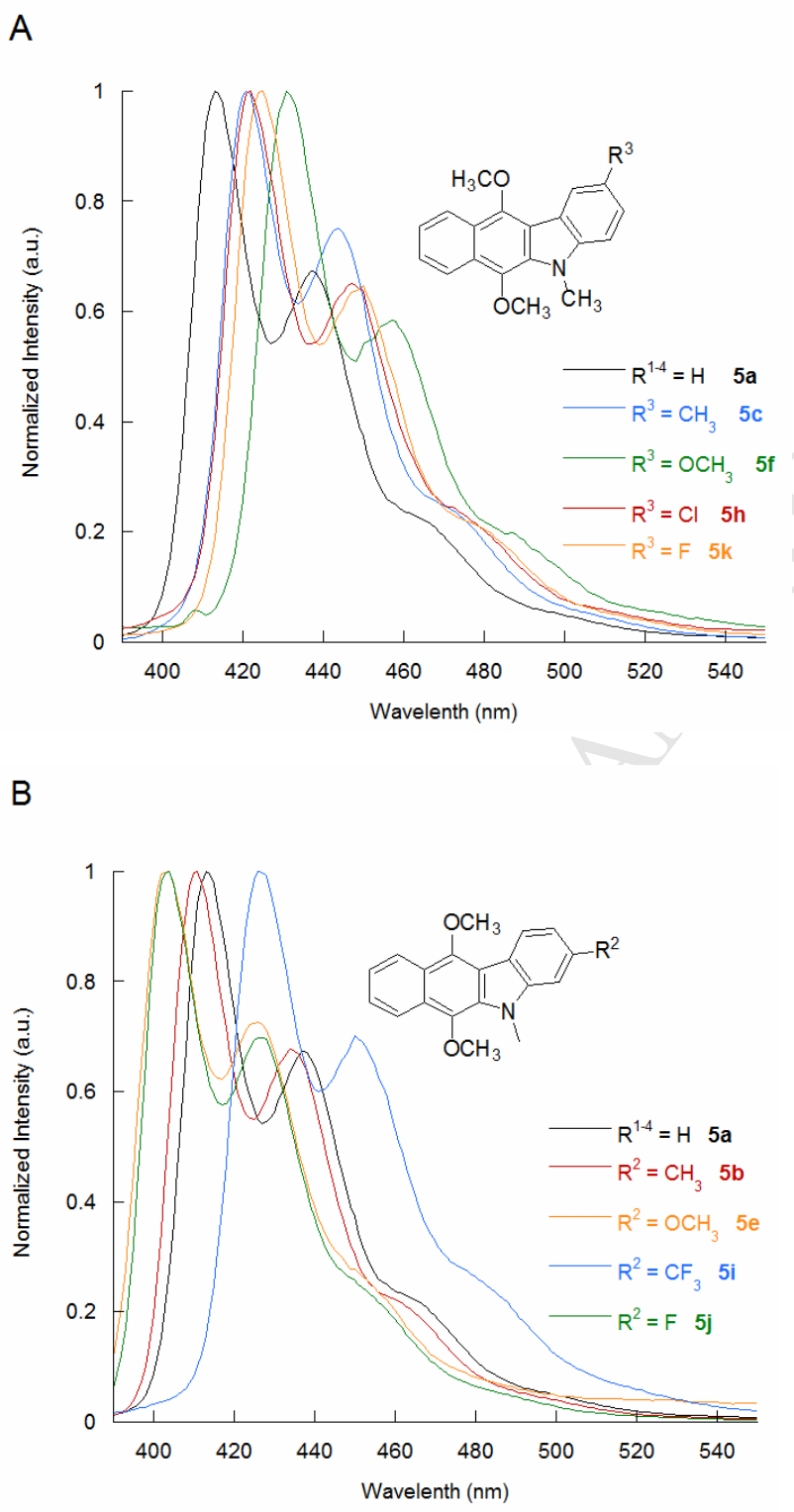

Figure 7: Part A. Normalized emission spectra of **5a** and derivatives with a substituent at R^3 in cyclohexane (λ_{exc} = 370 nm). Part B. Normalized emission spectra of **5a** and derivatives with a substituent at R^2 in cyclohexane (λ_{exc} = 370 nm).

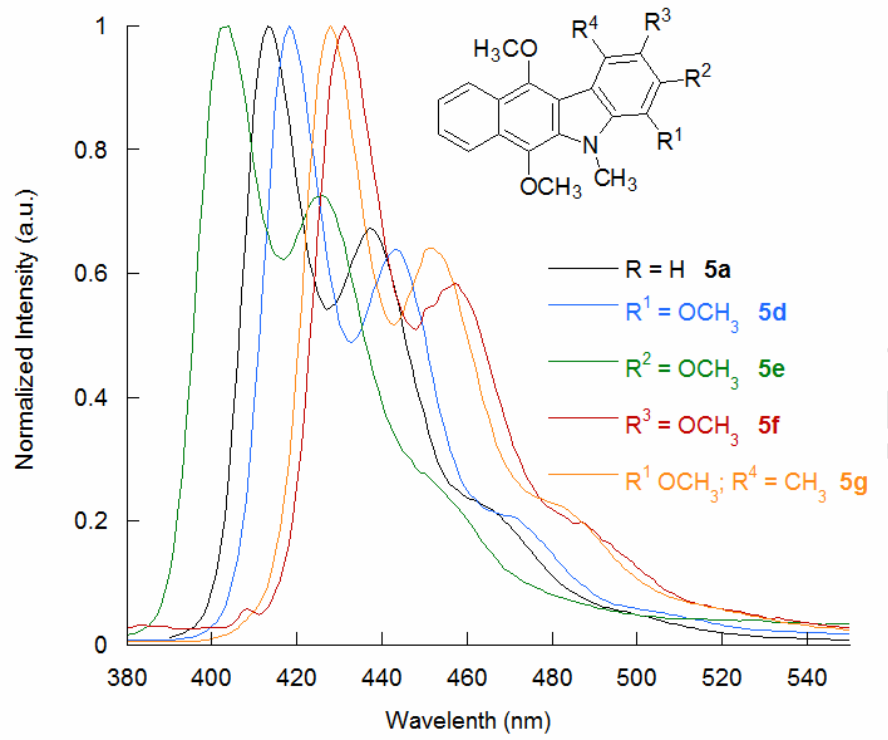

Figure 8: Normalized emission spectra of **5a** and compounds with methoxy substituent in cyclohexane. For **5a**, **5d**, **5g** and **5f** (λ_{exc} = 370 nm) and for **5e** (λ_{exc} = 365 nm).

The fluorescence emission spectra of the substituted benzocarbazole derivatives **5** preserve the substituent effect observed in the absorption spectra and values of λ_{max} emission are linearly red shifted relative to λ_{max} for absorption in cyclohexane (Figure 9). The change of solvent from cyclohexane to acetonitrile results in a greater variation of the larger Stokes shifts, although a similar tendency is observed to cyclohexane as solvent. The subtle differences in stabilization of both S_0 and S_1 for each compound in the polar solvent may be responsible for the greater variation of the observed Stokes shifts (Figure 9).

In comparison with substituted carbazole derivatives,[13b] the emission from compounds **5** is more than 50 nm red shifted whilst comparison with the parent

heterocycle **6**[14a] reveals that the introduction of the 6,11-dimethoxy substituents results in an approximately 30 nm red shift in the emission spectra. Further, the emission maxima of **5** are very similar to the recently reported 6,11-diphenylbenzo[2,3-*b*]carbazole derivatives.[14b]

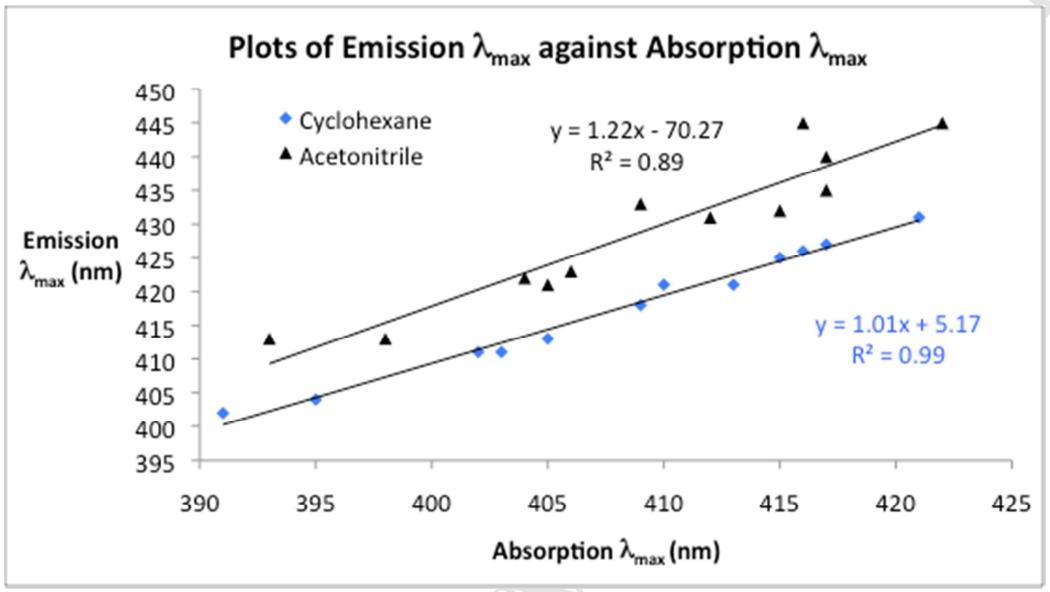

Figure 9. Graphical analysis of emission λ_{max} against absorption λ_{max} for **5**.

3.4 Quantum yield and fluorescence lifetime measurements

Table 3 details the quantum yields for **5** measured in four air saturated solvents of different polarities. The fluorescence quantum yield (Φ_f) for **5a** is similar to that of *N*-methylcarbazole (Φ_f 0.48 deoxygenated Cyh, 0.37 air saturated Cyh)[13b] and to 6,11-diphenylbenzo[2,3-*b*]carbazole (Φ_f 0.50 in DCM).[14b] Further, the fluorescence quantum yields for the derivatives of **5** vary in function of the substituents and the solvents (Table 3). Within the error of the experiment, the fluorescence quantum yields in MeOH are systematically smaller than in the non-protic solvents and Φ_f in CH_2Cl_2 is generally the largest or similar to Φ_f in cyclohexane. The smallest values of Φ_f are observed with **5g** (R^1=MeO,R^4=Me) and

5h (R^3=Cl). The reduced Φ_f of **5g** and **5h** maybe due to enhanced internal conversion as a result of the increased number of substituents with rotational freedom in the former and possibly spin-orbit coupling in the latter. On the other hand the largest values of Φ_f are observed for **5a** (ACN) and **5b** (CH_2Cl_2). The fluorescence lifetimes of **5** were measured using air and argon saturated samples. As can be seen for **5a** in figure 10 and for the other compounds in table 3, the presence of oxygen decreases the respective fluorescence lifetime of each compound. The fluorescence quenching by oxygen maybe due to a number of mechanistic possibilities.[30] Interestingly, under air saturated conditions the longest fluorescence lifetimes are observed in CH_2Cl_2. In the absence of oxygen the fluorescence lifetimes are slightly longer in the polar ACN and MeOH solvents reflecting the increased stability of the more polar lowest singlet excited state.

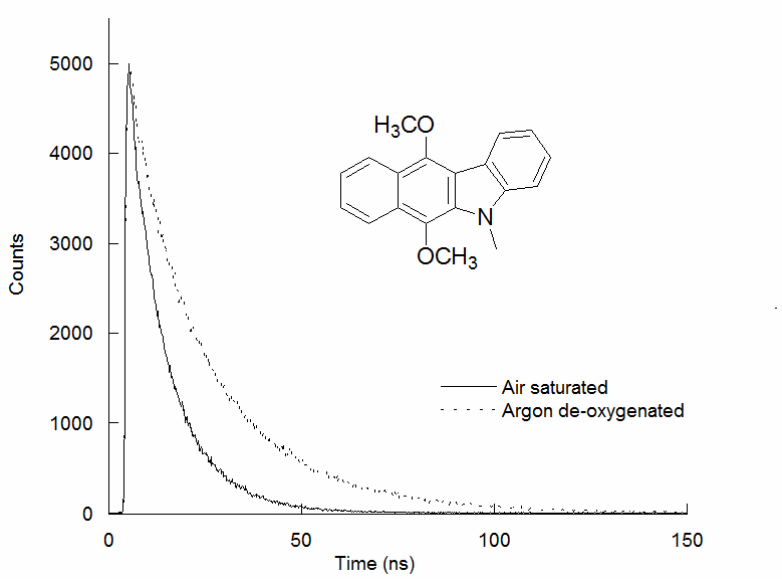

Figure 10: Fluorescence lifetime determination for **5a** in cyclohexane for an air saturated sample (—) and for a de-oxygenated, argon saturated, sample (· · ·).

Table 3: Fluorescence emission photophysical properties: Fluorescence quantum yield, lifetime, k_f e Σk_{nr} of **5a-k**.

	Cyh				DCM				ACN				MeOH			
Sample	Φ_f [a]	τ (ns) [b,c]	k_f [d]	$\sum k_{nr}$ [d]	Φ_f [a]	τ (ns) [b,c]	k_f [d]	$\sum k_{nr}$ [d]	Φ_f [a]	τ (ns) [b,c]	k_f [d]	$\sum k_{nr}$ [d]	Φ_f [a]	τ (ns) [b,c]	k_f [d]	$\sum k_{nr}$ [d]
5a	0.46	24.58 (10.22)	4.50	5.28	0.41	23.19 (14.86)	2.76	3.97	0.55	29.77 (9.76)	5.64	4.61	0.39	28.72 (11.13)	3.50	5.48
5b	0.40	20.62 (9.64)	4.15	6.22	0.57	21.98 (10.78)	5.29	3.99	0.42	25.81 (9.27)	4.53	6.26	0.34	22.88 (9.46)	3.59	6.98
5c	0.37	24.59 (10.24)	3.61	6.15	0.48	27.56 (15.80)	3.04	3.29	0.28	31.06 (9.88)	2.83	7.29	0.28	29.78 (11.21)	2.50	6.42
5d	0.39	21.82 (9.35)	4.17	6.52	0.44	22.01 (14.02)	3.14	3.99	0.40	26.71 (10.10)	3.96	5.94	0.39	25.24 (10.94)	3.56	5.58
5e	0.35	14.26 (7.98)	4.39	8.15	0.39	12.06 (8.69)	4.49	7.02	0.33	19.13 (8.17)	4.04	8.20	0.27	18.33 (9.09)	2.97	8.03
5f	0.30	24.09 (9.89)	3.03	7.08	0.42	27.12 (15.04)	2.79	3.86	0.39	30.98 (10.37)	3.76	5.88	0.31	30.71 (11.60)	2.67	5.95
5g	0.23	17.6 (8.78)	2.62	8.77	0.31	17.55 (11.53)	2.69	5.98	0.26	24.21 (9.18)	2.83	8.06	0.25	21.48 (9.98)	2.51	7.52

5h	0.18	21.19 (10.51)	1.71	7.80	0.16	23.19 (14.16)	1.13	5.93	0.11	26.80 (9.65)	1.14	9.22	0.17	25.90 (9.93)	1.71	8.36
5i	0.35	25.96 (11.88)	2.95	5.47	0.36	25.76 (15.64)	2.30	4.09	0.39	31.20 (11.33)	3.44	5.38	0.26	28.57 (12.75)	2.04	5.80
5j	0.36	23.31 (10.12)	3.56	6.32	0.45	21.24 (14.52)	3.10	3.79	0.27	25.19 (11.63)	2.32	6.28	0.34	24.44 (12.76)	2.66	5.17
5j'	0.38	24.05 (10.37)	3.66	5.98	0.41	21.97 (13.39)	3.06	4.41	0.26	25.01 (11.32)	2.30	6.54	0.33	24.44 (11.24)	2.94	5.96
5k	0.39	25.01 (11.24)	3.47	5.43	0.37	23.22 (13.54)	2.73	4.65	0.34	25.30 (10.59)	3.21	6.23	0.33	26.73 (11.72)	2.82	5.72

a Air saturated samples.

b Values after 15 min de-oxygenated with argon. In parenthesis air saturated values.

c Excitation wavelength 404.2nm and emission wavelength 445nm.

d $k_f = \Phi_f / \tau$ (10^7/ s); $\Sigma k_{nr} = (1/\tau) - k_f$ (10^7/ s), calculated for air saturated sample.

3.5 Theoretical calculations

3.5.1 Calculation of absorption and emission spectra

Data with respect to the calculated UV-vis spectra for the parent 2,3-benzo[*b*]carbazole (**6**), *N*-methyl-6,11-dimethoxybenzo[*b*]carbazole (**5a**), derivatives **5b-k**, as well as the **nor-5a-k** derivatives (*N*-hydrogen instead of *N*-methyl) are presented in table 4 (and SI Tables 14 and 15). Data referring to calculated fluorescence spectra are given in table 5. The UV-vis spectra of **6** (experimental λ_{max} 383 nm)[14a] and **nor-5a** were calculated using a number of commonly used TD-DFT methods (B3LYP, CAM-B3LYP, PBE0, ωd97xd). The long range correction hybrids (CAM-B3LYP and ωB97XD) gave enormously ultra-violet shifted spectra whereas the global hybrids B3LYP and PBE0 gave spectral predictions of the $\lambda_{0,0}$ transition for the first excited state (ES) much closer to the experimentally observed S_0-S_1 maximum of **5a** and **6**.[31] The former being consistently closer to the experimentally observed maxima in comparison to the latter, which are marginally blue shifted. The inclusion of implicit solvation (IEF-PCM, solvent=cyclohexane or acetonitrile)[32] in the calculation of the UV-vis spectrum of **5a** resulted in a lowering of the energies of the calculated transitions, consistent with solvent stabilization, and reproduced the small bathochromic shift on passing from the apolar cyclohexane to the polar acetonitrile solvent. Calculation of the UV-vis spectra in the following manner TD-X/6-31+G(d)//B3LYP/6-31+G(d) (X = PBE0 or CAM-B3LYP) resulted in a bathochromic shift of the $\lambda_{0,0}$ transition for excitation to the first ES in comparison to the respective calculations based upon geometries optimized with the X density functional. However, the results remained blue shifted in comparison to the use of TD-B3LYP. Calculation of the UV-vis spectra of **5a** revealed that the *N*-methyl derivative is red shifted by 10 nm in comparison to the *N*-hydrogen **nor-5a**. Further,

the incorporation of implicit solvation through the IEF-PCM model resulted in an additional red shift of the $\lambda_{0,0}$ transition for the excitation $S_0 \rightarrow S_1$ such that the predicted value of the $\lambda_{0,0}$ transition was now less than 15 nm (aprox. 0.10 eV) blue shifted from the observed value for λ_{max}. The large difference in the results for the use of the long range correction hybrids (CAM-B3LYP and ωB97XD) most likely reflects that vertical excitation of **5** or **6** does not involve a very delocalized charge transfer excited state.[33]

Table 4: Calculation of UV-vis spectra: Vertical transitions for the first two lowest energy singlet excited states and the subsequent two singlet excited states with the largest oscillator strengths.[a]

Compound (TD)-DFT Method	Excited state (ES): Vertical transition energies (eV, nm) Oscillator strength (f)			
6 - B3LYP	ES 1: 3.3546 eV	ES 2: 3.9034 eV	ES 4: 4.5079 eV	ES 7: 4.9450 eV
Exp.: 383 nm[14a]	369.59 nm	317.63 nm	275.04 nm	250.73 nm
	f=0.0408	f=0.0622	f=0.4732	f=0.5600
6 - PBE0	ES 1: 3.4693 eV	ES 2: 4.0269 eV	ES 4: 4.6550 eV	ES 7: 5.1319 eV
	357.38 nm	307.89 nm	266.35 nm	241.60 nm
	f=0.0447	f=0.0688	f=0.7668	f=0.5124
6 – CAM-B3LYP	ES 1: 3.8048 eV	ES 2: 4.2669 eV	ES 3: 4.8582 eV	ES 5: 5.1827 eV
	325.86 nm	290.57 nm	255.20 nm	239.23 nm
	f=0.0573	f=0.0975	f=0.3949	f=1.0986
6 - ωB97XD	ES 1: 3.8421 eV	ES 2: 4.2970 eV	ES 3: 4.8835 eV	ES 4: 5.2464 eV
	322.70 nm	288.54 nm	253.88 nm	236.32 nm
	f=0.0582	f=0.0961	f=0.3815	f=1.2254
nor-5a –	ES 1: 3.2684 eV	ES 2: 3.8482 eV	ES 3: 4.3995 eV	ES 7: 4.8282 eV
B3LYP	379.34 nm	322.19 nm	281.81 nm	256.79 nm
	f=0.0695	f=0.0067	f=0.5577	f=0.6006
nor-5a –	ES 1: 3.7223 eV	ES 2: 4.2331 eV	ES 3: 4.8275 eV	ES 5: 5.1215 eV
CAM-B3LYP	333.09 nm	292.89 nm	256.83 nm	242.09 nm
	f=0.0984	f=0.0147	f=0.4859	f=1.0436
nor-5a –	ES 1: 3.3775 eV	ES 2: 3.9719 eV	ES 3: 4.5636 eV	ES 7: 5.0402 eV
PBE0	367.08 nm	312.15 nm	271.68 nm	245.99 nm

	f=0.0752	f=0.0064	f=0.6853	f=0.6640
nor-5a –	ES 1: 3.7595 eV	ES 2: 4.2630 eV	ES 3: 4.8586 eV	ES 4: 5.1762 eV
ωB97XD	329.79 nm	290.84 nm	255.18 nm	239.53 nm
	f=0.1004	f=0.0140	f=0.4609	f=1.1388
nor-5a –	ES 1: 3.2307 eV	ES 2: 3.8364 eV	ES 3: 4.3121 eV	ES 6: 4.7439 eV
B3LYP	383.76 nm	323.18 nm	287.53 nm	261.36 nm
IEFPCM-Cyh	f=0.0947	f=0.0089	f=1.0838	f=0.4950
nor-5a –	ES 1: 3.2126 eV	ES 2: 3.8292 eV	ES 3: 4.3264 eV	ES 6: 4.7615 eV
B3LYP	385.93 nm	323.79 nm	286.57 nm	260.39 nm
IEFPCM-ACN	f=0.0878	f=0.0065	f=1.0087	f=0.4859
nor-5a –	ES 1: 3.6222 eV	ES 2: 4.1557 eV	ES 3: 4.6937 eV	ES 4: 4.9493 eV
CAM-B3LYP//B3LYP	342.29 nm	298.35 nm	264.15 nm	250.51 nm
	f=0.1364	f=0.0245	f=1.1976	f=0.8134
nor-5a –	ES 1: 3.3243 eV	ES 2: 3.9391 eV	ES 3: 4.4446 eV	ES 7: 4.9640 eV
PBE0//B3LYP	372.96 nm	314.75 nm	278.95 nm	249.77 nm
	f=0.1024	f=0.0098	f=1.2809	f=0.3749
5a – B3LYP	ES 1: 3.1913 eV	ES 2: 3.7850 eV	ES 3: 4.3535 eV	ES 7: 4.7831 eV
Exp. 405 nm	388.51 nm	327.57 nm	284.79 nm	259.21 nm
	f=0.0630	f=0.0027	f=0.6234	f=0.4868
5a – B3LYP	ES 1: 3.1538 eV	ES 2: 3.7735 eV	ES 3: 4.2557 eV	ES 7: 4.7358 eV
IEFPCM-Cyh	393.13 nm	328.57 nm	291.34 nm	261.80 nm
Exp. 405 nm	f=0.0861	f=0.0036	f=1.1500	f=0.6931
5a – B3LYP	ES 1: 3.1318 eV	ES 2: 3.7660 eV	ES 3: 4.2679 eV	ES 7: 4.7476 eV
IEFPCM-ACN	395.88 nm	329.22 nm	290.51 nm	261.15 nm
Exp. 406 nm	f=0.0790	f=0.0038	f=1.0588	f=0.7650

[a] Calculation method: (IEFPCM)-TD-DFT/6-31+G(d)//(IEFPCM)-DFT/6-31+G(d). TD-DFT calculations nstates=20.

The effect of introduction of a methoxy group at positions R^1 to R^4 on the phenylene ring of **nor-5a** was also calculated. The results are detailed in SI Table 14 and reveal a systematic effect upon the value of $\lambda_{0,0}$ for the $S_0 \rightarrow S_1$ transition relative to the unsubstituted **nor-5a** that is dependent upon the position of the substituent in an analogous manner to the experimentally observed results for **5**, ie. substitution at position R^1 or R^3 (Scheme 1) results in a bathochromic shift whilst substitution at positions R^2 or R^4 result in a hypsochromic shift for an electron donating substituent.

The faithful reproduction of the substituent effect prompted the calculation of the UV-vis spectra for **5a-k** (SI Table 15) and the results for the calculated $\lambda_{0,0}$ for the $S_0 \rightarrow S_1$ transition are graphically portrayed in figure 11. As can be seen from figure 11, the substituent effect (irrespective of position, R^1–R^4, or electron donating or withdrawing nature) is effectively simulated in the calculations.

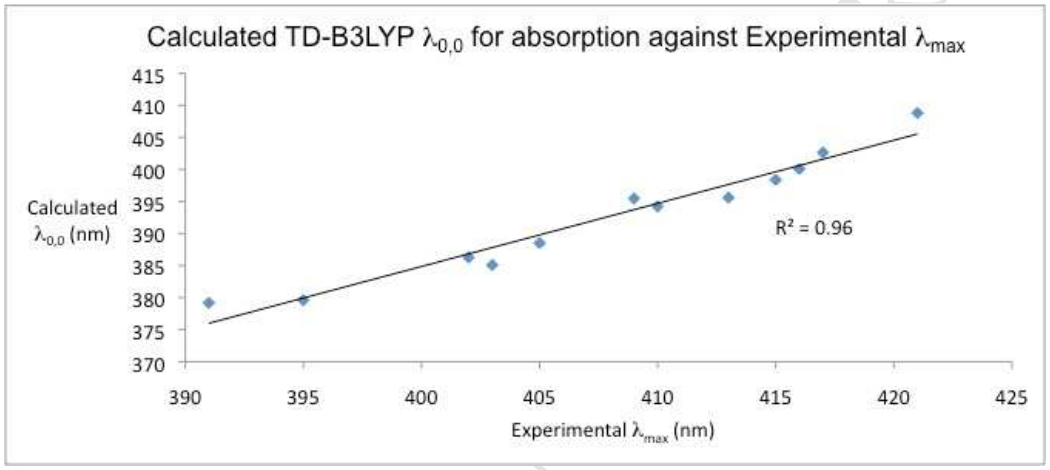

Figure 11. Comparison of the calculated (gas phase TD-B3LYP/6-31+G(d)//B3LYP/6-31+G(d), nstates=20) values for $\lambda_{0,0}$ for the $S_0 \rightarrow S_1$ transition with the experimentally observed value of λ_{max} (cyclohexane) for compounds **5**.

Additionally, the results for the first two excited states and the subsequent two excited states with the largest oscillator strengths reproduce the minimal features of the experimental spectra (Figure 12). Notably, in comparison to the parent heterocycle (**6**), the second excited state of **5** has an oscillator strength smaller than the first excited state as also experimentally verified by comparison with the spectrum of **6**.[13a]

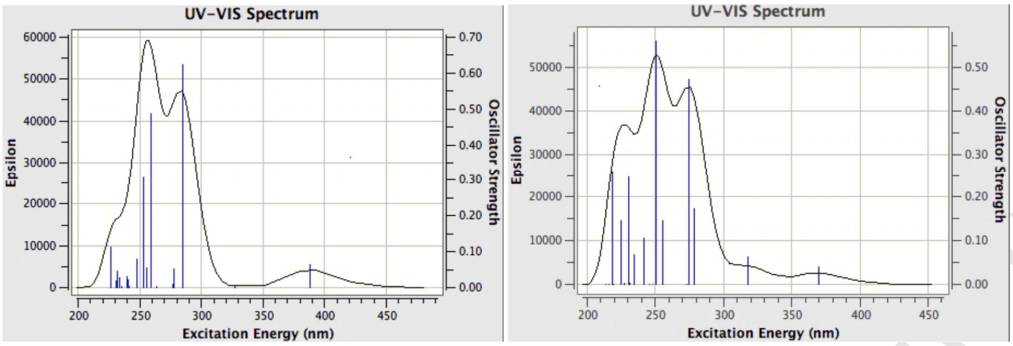

Figure 12. TD-B3LYP (nstates=20) calculated UV-vis spectra of compounds **5a** (left) and **6** (right).

The fluorescence emission ($\lambda_{0,0}$) was calculated for **6** and **nor-5a**. For the latter compound implicit solvation (IEFPCM) was also taken into consideration.[34] The results are presented in table 4. For **6**, it can be seen that the use of the TD-PBE0 functional gave an excellent prediction for $\lambda_{0,0}$ emission and the respective TD-B3LYP result was red shifted by 11 nm. In the case of **nor-5a** the effect of implicit solvation was evaluated. As seen in the calculation for **6**, the TD-B3LYP results for **nor-5a** are red shifted by approximately 11 nm with respect to the TD-PBE0 results. The inclusion of implicit solvation in the calculation, relative to the gas phase result, gives a small red shift (3 nm) for cyclohexane and a slightly larger red shift for acetonitrile (about 10-12 nm) independent of the density functional used for the calculation. In addition, the gas phase $\lambda_{0,0}$ emission was calculated using TD-PBE0 for examples of compounds **5** (Table 5). The results are compared with the experimental values of λ_{max} for emission in cyclohexane. The calculated gas phase values accurately (within aprox. 0.05 eV) reproduce the experimentally observed differences in the emission spectra of the variously substituted derivatives of **5**.

Table 5: Calculated values for $\lambda_{0,0}$ emission from **6**, and examples of **5**, and comparison with experimental values of λ_{max} emission.

Fluorescence calc. method[a]	*TD-B3LYP*	*IEFPCM-TD-B3LYP-Cyh*	*IEFPCM-TD-B3LYP-ACN*	*TD-CAM-B3LYP*	*TD-PBE0*	*IEFPCM-TD-PBE0-Cyh*	*IEFPCM-TD-PBE0-ACN*
Compound							
6	3.1103 eV				3.2141 eV		
	398.62 nm				385.76 nm		
	387 nm[b]				387 nm[b]		
nor-5a	2.9438 eV	2.9227 eV	2.8620 eV	3.3087 eV	3.0256 eV	3.0040 eV	2.9473 eV
	421.17 nm	424.21 nm	433.21 nm	374.72 nm	409.79 nm	412.72 nm	420.67 nm
*Compound **(N-Me)***	**5a**	**5d**	**5e**	**5e'**	**5f**	**5g**	**5i**
Fluorescence calc. method[a]							
TD-PBE0	3.0074 eV	2.9255 eV	3.0833 eV	3.0103 eV	2.8546 eV	2.8618 eV	2.8652 eV
	412.27 nm	423.80 nm	402.12 nm	411.87 nm	434.33 nm	433.23 nm	432.72 nm
Experimental[c]	413 nm	418 nm	402 nm		431 nm	427 nm	426 nm

[a] Optimization: (IEFPCM)-(TD)-DFT/6-31+G(d), for the optimized TD-DFT calculations nstates=10.

[b] Value taken from reference[14a]

[c] This study, experimental values given are those recorded in cyclohexane as solvent.

3.5.2 Charge distribution in the ground and lowest lying excited states

A comparison of the charge distribution in the ground and the lowest energy singlet excited states for **nor-5a** and **6**, where the total electronic density was divided into the naphthylene, phenylene and substituted nitrogen structural units, is detailed in table 6.[35]

Table 6. Calculated ChelpG ([TD]-DFT) charges summed over all atoms for structural units of S_0, S_1 and S_2 states of compounds **6** and **nor-5a**.[a]

	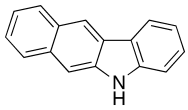 **6**			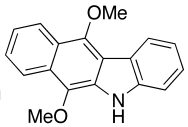 **nor-5a**		
Structural fragment	GS (S_0)	ES (S_1)	ES (S_2)	GS (S_0)	ES (S_1)	ES (S_2)
Naphthylene[b]	0.1180	0.0294	0.0791	-0.1251	-0.1474	-0.1527
Phenylene[b]	0.1541	0.1296	0.2188	0.1619	0.1584	0.1955
HN[b]	-0.2721	-0.1591	-0.2979	-0.0368	-0.0109	-0.0428
Naphthylene[c]	0.1094	0.0255	0.0872	-0.1193	-0.1451	-0.1430
Phenylene[c]	0.1562	0.1337	0.2170	0.1676	0.1428	0.1989
HN[c]	-0.2655	-0.1591	-0.3042	-0.0483	0.0023	-0.0559

[a] Values are given in electrons (e). A positive value reflects a relative electron density deficiency whilst a negative value reflects a relative excess of electron density. Any deviation from a total difference in electron density other than zero is a consequence of reducing the number of significant figures.

[b] (TD)B3LYP/6-31+G(d).

[c] (TD)PBE0/6-31+G(d).

Comparison of the fragmented electrostatic potentials of the optimized S_0, S_1 and S_2 states reveals changes in the overall distribution of electronic charge associated

with the excited states relative to the ground state. Notably for the parent heterocyclic system **6**, the NH group has an excess of electron density as a consequence of the electronegativity of the nitrogen, whereas the aromatic units (naphthylene and phenylene) are less electron rich relative to the NH group with its lone pair. Excitation to the first excited state results in a redistribution of the electron density from the NH group to the aromatic units, principally the naphthlyene unit. S_2 of **6** is characterized by a considerable loss of electron density from the phenylene unit to the naphthylene unit and the NH group. Thus S_1 represents a short range redistribution of electron density from nitrogen to principally the naphthlyene unit whilst S_2 represents a greater charge reorganization between the aromatic units due to charge transfer from the phenylene unit to the NH and naphthylene units.

The introduction of the methoxy substituents on the naphthylene unit has the effect of increasing the ground state electron density within the naphthylene unit and at the same time moderates the polarizing effect of the NH group. The phenylene group is also less electron rich in comparison to the naphthylene and NH groups. For **nor-5a**, excitation to S_1 parallels the electronic distribution seen in **6**. The NH group losses electron density and the naphthylene and phenylene groups have greater electron density relative to the ground state. Further, in a similar manner to **6**, excitation to S_2 involves electron density loss from the phenylene unit to the naphthylene and NH groups. Thus the electronic transitions to S_1 and S_2 of **nor-5a** are in essence similar to those observed for **6**. However, the magnitude of the changes in electronic density within the structural fragments is considerably smaller for **nor-5a** in comparison to **6**.

Table 7: Calculated ChelpG ([TD]-PBE0) charges summed over all atoms for structural units of S_0 and S_1 states of selected **5**.[a]

Structure	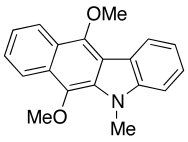		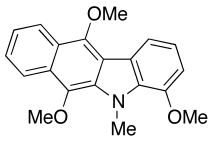		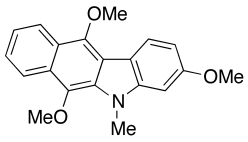	
5	S_0 **5a**	S_1	S_0 **5d**	S_1	S_0 **5e**	S_1
Nap[b]	-0.1924	-0.2627	-0.2093	-0.3868	-0.2214	-0.2993
Phen[b]	0.0967	0.0962	0.0344	0.0783	0.0488	0.0631
NMe[b]	0.0957	0.1664	0.1748	0.3085	0.1726	0.2361
Structure	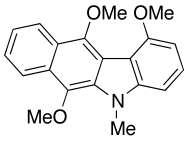		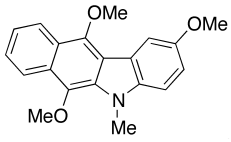		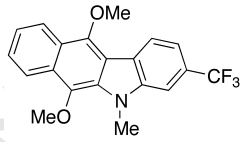	
5	S_0 **5e'**	S_1	S_0 **5f**	S_1	S_0 **5i**	S_1
Nap[b]	-0.1659	-0.1988	-0.2143	-0.3709	-0.1522	-0.0807
Phen[b]	0.0298	0.0359	0.0547	0.0942	0.0465	-0.0916
NMe[b]	0.1361	0.1629	0.1596	0.2767	0.1058	0.1723

[a] (TD)PBE0/6-31+G(d). Values are given in electrons (e). A positive value reflects a relative electron density deficiency whilst a negative value reflects a relative excess of electron density. Any small discrepancy from a total difference in electron density other than zero is a consequence of reducing the number of significant figures.

[b] Nap = dimethoxynaphthylene unit, Phen = substituted phenylene unit, NMe = *N*-methyl unit.

The calculated charges for the ground and first excited states of selected examples of compounds **5** are detailed in table 7 and color coded MEPs of S_0 and S_1 for compounds **5a**, **5f** and **5i** are shown in figure 13. For compounds **5d-f**, the presence of the additional MeO group bonded to the phenylene ring fragment on the excitation $S_0 \rightarrow S_1$ results in a displacement of electron density from the phenylene and

nitrogen groups to the naphthylene fragment. For the methoxyphenylene derivatives the largest displacement of charge occurs with **5f** followed by **5d** where the methoxy substituents occupy the positions R^3 and R^1 respectively. In contrast, the calculated structure for S_1 of compound **5i** clearly indicates an inversion of the electronic transition that results in the loss of electron density from the naphthylene and the NMe units to the phenylene unit.

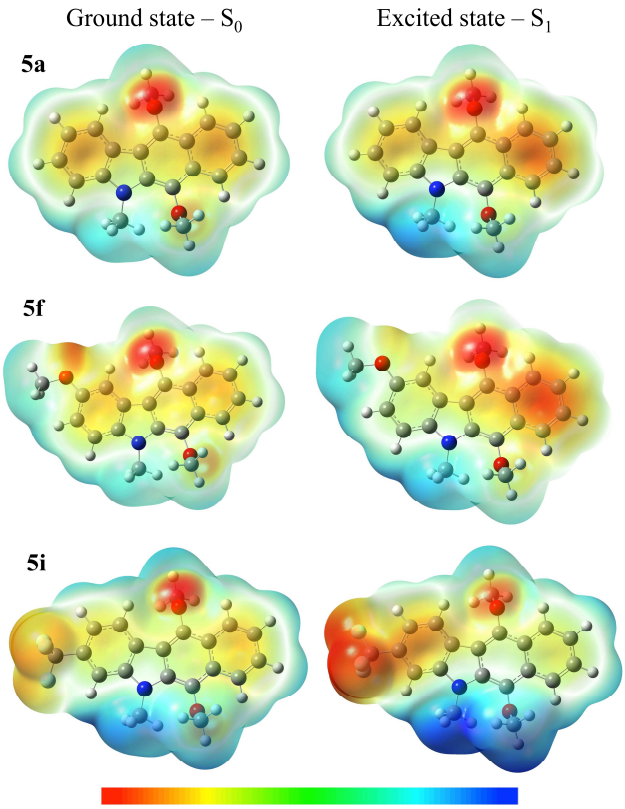

Figure 13. Color coded maps of electrostatic potential (ChelpG) for S_0 and S_1 of **5a**, **5f** and **5i** (blue is positive and red is negative).

Evaluation of the charge density by comparison of the ground and first excited state MEPs allows for rationalization of the substituent effects upon the absorption spectra of **5**. Figure 14 depicts a cartoon representation of the differences in electron density of the first excited state for **5** with electron donating or electron withdrawing

substituents at positions $R^{1,3}$ or $R^{2,4}$ respectively. The charge delocalization in the excited state is stabilized by the respective substituents and leads to a bathochromic shift of the absorption spectra and a more relaxed excited state in polar solvents. The inverse situation is less well defined due to the limited number of examples in the present study and requires further study. However, when electron donating substituents occupy positions $R^{2,4}$ the electronic transition to S_1 is destabilized relative to **5a** (a blue shift occurs). This can be attributed to the inability of these substituents to stabilize the electron density deficiency on nitrogen as a consequence of the electronic transition to S_1. Further, it can be speculated that the incorporation of strongly electron withdrawing groups at positions $R^{1,3}$ will also result in bathochromic shifts due to a change in the nature of the electronic transition.

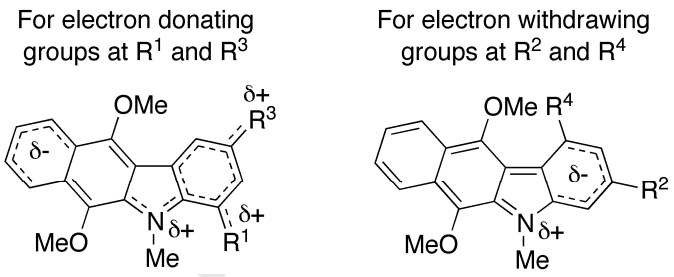

Figure 14. Cartoon representations of electron density distribution in S_1 as a function of the electronic properties of the substituents R^{1-4}.

4. Conclusion

A selection of novel 6,11-dimethoxy-5(*N*)-methylbenzo[*b*]carbazole derivatives (**5**) were prepared in a concise manner from anilines (**1**) and naphthoquinone (**2**) by use of consecutive catalytic oxidative C-H functionalization reactions followed by a one pot reductive methylation of the intermediates **4**. The absorption and fluorescence emission properties of the novel structures were

characterized in solvents of different polarities. Small Stokes shifts were observed in cyclohexane whilst marginally larger values were observed in CH_2Cl_2 and principally the polar solvents ACN and MeOH reflecting stabilization of the lowest excited state in the polar solvents. The increased stabilization of the lowest excited state in the polar solvents was also verified by the longer fluorescence lifetimes of **5** in the polar solvents. Compounds **5** displayed reasonably large fluorescence quantum yields and might be interesting biological probes. The position and nature of the substituents R^{1-4} were found to influence the spectroscopic properties of **5**. Time dependent density functional theory calculations were used to characterize the absorption and fluorescence emission spectra of **5**. An excellent correlation of the calculated absorption properties was obtained through the use of the B3LYP functional whilst the emission properties were faithfully reproduced through the use of the PBE0 functional. That the global hybrids gave the best predictions of values for $\lambda_{0,0}$ reflects the nature of the π-π^* electronic transition for both absorption and emission where the extent of charge delocalization is relatively small. The calculation of the electrostatic potential for S_0 and S_1 allowed comparison of the overall electron density distribution in the two states for differently substituted derivatives of **5**. An inversion of the electronic transition dipole moment was observed when the strongly electron withdrawing substituent R^2 = CF_3 (**5i**) was present and this accounted for the moderate bathochromic shift of this substituent in polar solvents similar to that seen for R^3 = MeO (**5f**) although for a different reason. The latter compound reveals a moderate bathochromic shift due to resonance stabilization of the electron density shift to the naphthylene unit in contrast to **5i**. The analysis of the experimental and theoretical data point to the possibility of the designed control of the excited state properties of judiciously substituted derivatives of **5**.

Acknowledgments

The authors thank CNPq, CAPES and FAPERJ for financial assistance and the mass spectroscopy facilities at IPPN-UFRJ and at the Fundação Oswald Cruz, Rio de Janeiro.

Supporting Information

Spectroscopic characterization of **4** as well as details of the preparation and the spectra for structural characterization of **5**. Absorption, emission and excitation spectra of compounds **5** and tables of calculated vertical excitations of **nor-5** and **5**.

References

[1] Graebe C. Ueber Synthesen des Carbazols. Ber Deut Chem Ges. 1872;5:376-8.

[2] Chakraborty DP, Barman BK, Bose PK. Constitution of murrayanine, a carbazole derivative isolated from Murraya koenigii. Tetrahedron. 1965;21:681-5.

[3] [a] Knoelker H-J, Reddy KR. Isolation and Synthesis of Biologically Active Carbazole Alkaloids. Chem Rev 2002;102:4303-427; [b] Schmidt AW, Reddy KR, Knoelker H-J. Occurrence, Biogenesis, and Synthesis of Biologically Active Carbazole Alkaloids. Chem Rev 2012;112:3193-328; [c] Tan S-P, Nafiah MA, Ahmad K. C23-carbazole alkaloids from malayan Murraya koenigii (L.) spreng. J Chem Pharm Res. 2014;6:1093-8; [d] Knoelker H-J. Synthesis of biologically active carbazole alkaloids using selective transition-metal-catalyzed coupling reactions. Chem Lett. 2009;38:8-13; [e] Forke R, Gruner KK, Knott KE, Auschill S, Agarwal S, Martin R, et al. Transition metals in organic synthesis. 93. Total synthesis of biologically active alkaloids using transition metals. Pure Appl Chem. 2010;82:1975-91.

[4] [a] Nandy BC, Gupta AK, Mittal A, Vyas V. Carbazole: it's biological activity. J Biomed Pharm Res. 2014;3:42-8; [b] Gluszynska A. Biological potential of carbazole derivatives. Eur J Med Chem. 2015;94:405-26.

[5] [a] Johnson GE. Fluorescence quenching of carbazoles. J Phys Chem. 1980;84:2940-6; [b] Shao H, Chen X, Wang Z, Lu P. Synthesis and fluorescence properties of carbazole and fluorene-based compounds. J Lumin. 2007;127:349-54; [c] Wu J-Y, Pan Y-L, Zhang X-J, Sun T, Tian Y-P, Yang J-X, et al. Synthesis, photoluminescence and electrochemical properties of a series of carbazole-functionalized ligands and their silver(I) complexes. Inorg Chim Acta. 2007;360:2083-91; [d] Blouin N, Leclerc M. Poly(2,7-carbazole)s: Structure-Property Relationships. Acc Chem Res. 2008;41:1110-9; [e] Lellouche J-P, Koner RR, Ghosh S. N-Substituted carbazole heterocycles and derivatives as multipurpose chemical species: at the interface of chemical engineering, polymer and materials science. Rev Chem Eng. 2013;29:413-37; [f] Bahy A, Chemli M, Hassine BB. Synthesis and characterization of new carbazole-based materials for optoelectronic applications. Tetrahedron Lett. 2013;54:4026-9; [g] Kong L, Wang Z, Zhao J, Xu J. Multi-electrochromic 2,7-linked polycarbazole derivative and its application in electrochromic devices. Int J Electrochem Sci. 2015;10:982-96; [h] Adhikari RM, Neckers DC, Shah BK. Photophysical study of blue, green, and orange-red light-emitting carbazoles. J Org Chem. 2009;74:3341-9; [i] Kirkus M, Simokaitiene J, Grazulevicius JV, Jankauskas V. Phenyl-, carbazolyl- and fluorenyl-substituted derivatives of indolo[3,2-b]carbazole as hole-transporting glass forming materials. Synth Met. 2010;160:750-5; [j] Asiri AM, Khan SA, Al-Amoudi MS, Alamry KA. Synthesis, characterization, absorbance, fluorescence and nonlinear optical properties of some donor acceptor chromophores. Bull Korean Chem Soc. 2012;33:1900-6; [k] Sigwalt P, Wegner G, Morin J-F, Leclerc M, Ades D, Siove A. Polycarbazoles: 25 years of progress. Macromol Rapid Commun. 2005;26:761-78; [l] Zhang L, Zhou J, Zhang L. Synthesis and fluorescent properties of carbazole-substituted hydroxyethyl celluloses. Macromol Chem Phys. 2012;213:57-63; [m] Zhang Q, Zhu W, Fang M, Yin F, Li C. Synthesis, photophysical and electrochemical properties of two novel carbazole-based dye molecules. Spectrochim Acta, Part A. 2015;135:379-85.

[6] [a] Bagnich SA, Rudnick A, Schroegel P, Strohriegl P, Koehler A. Triplet energies and excimer formation in meta- and para-linked carbazolebiphenyl matrix materials. Philos Trans

R Soc, A. 2015;373:1-8; [b] Lee CW, Lee JY. High quantum efficiency and color stability in white phosphorescent organic light emitting diodes using a pyridine modified carbazole derivative. Dyes Pigm. 2014;103:34-8; [c] Thomas KRJ, Lin JT, Tao Y-T, Ko C-W. Light-Emitting Carbazole Derivatives: Potential Electroluminescent Materials. J Am Chem Soc. 2001;123:9404-11; [d] Fu H-Y, Wu H-R, Hou X-Y, Xiao F, Shao B-X. N-Aryl carbazole derivatives for non-doped red OLEDs. Synth Met. 2006;156:809-14; [e] Van Dijken A, Bastiaansen JJAM, Kiggen NMM, Langeveld BMW, Rothe C, Monkman A, et al. Carbazole Compounds as Host Materials for Triplet Emitters in Organic Light-Emitting Diodes: Polymer Hosts for High-Efficiency Light-Emitting Diodes. J Am Chem Soc. 2004;126:7718-27; [f] Bagnich SA, Athanasopoulos S, Rudnick A, Schroegel P, Bauer I, Greenham NC, et al. Excimer Formation by Steric Twisting in Carbazole and Triphenylamine-Based Host Materials. J Phys Chem C. 2015;119:2380-7; [g] Jiang H, Sun J, Zhang J. A review on synthesis of carbazole-based chromophores as organic light-emitting materials. Curr Org Chem. 2012;16:2014-25; [h] Lu J, Xia PF, Lo PK, Tao Y, Wong MS. Synthesis and Properties of Multi-Triarylamine-Substituted Carbazole-Based Dendrimers with an Oligothiophene Core for Potential Applications in Organic Solar Cells and Light-Emitting Diodes. Chem Mater. 2006;18:6194-203; [i] Yin N, Feng L. A novel blue emission PLED material: synthesis, photophysical and electrochemical properties. Dyes Pigm. 2015;117:116-21; [j] Wang P, Fan H-L, He Y-B, Huang H-F, Zhu C-C, Gao X-C, et al. Small molecules with pyridine backbone modified with carbazole, fluorine and bromine for white light-emitting diode applications. Displays. 2013;34:320-5.

[7] [a] McGrath JE, Rasmussen L, Shultz AR, Shobha HK, Sankarapandian M, Glass T, et al. Novel carbazole phenoxy-based methacrylates to produce high-refractive index polymers. Polymer. 2006;47:4042-57; [b] Zhang Y, Wada T, Sasabe H. Carbazole photorefractive materials. J Mater Chem. 1998;8:809-28.

[8] [a] Chen L-X, Niu C-G, Zeng G-M, Huang G-H, Shen G-L, Yu R-Q. Carbazole as fluorescence carrier for preparation of doxycycline sensor. Anal Sci. 2003;19:295-8; [b] Feng XJ, Tian PZ, Xu Z, Chen SF, Wong MS. Fluorescence-Enhanced Chemosensor for Metal

Cation Detection Based on Pyridine and Carbazole. J Org Chem. 2013;78:11318-25; [c] Li P, Zhao Y, Yao L, Nie H, Zhang M. A simple, selective, fluorescent iron(III) sensing material based on peripheral carbazole. Sens Actuators, B. 2014;191:332-6; [d] Ortyl J, Galica M, Popielarz R, Bogdal D. Application of a carbazole derivative as a spectroscopic fluorescent probe for real time monitoring of cationic photopolymerization. Pol J Chem Technol. 2014;16:75-80.

[9] [a] Boudreault P-LT, Wakim S, Blouin N, Simard M, Tessier C, Tao Y, et al. Synthesis, Characterization, and Application of Indolo[3,2-b]carbazole Semiconductors. J Am Chem Soc. 2007;129:9125-36; [b] Boudreault P-LT, Virkar AA, Bao Z, Leclerc M. Synthesis and characterization of soluble indolo[3,2-b]carbazole derivatives for organic field-effect transistors. Organic Electronics. 2010;11:1649-59; [c] Zhang X, Chi Z, Yang Z, Chen M, Xu B, Zhou L, et al. Synthesis of carbazole derivatives with high quantum yield and high glass transition temperature. Opt Mater 2009;32:94-8.

[10] Illos RA, Shamir D, Shimon LJW, Zilbermann I, Bittner S. N-Dansyl-carbazoloquinone; a chemical and electrochemical fluorescent switch. Tetrahedron Lett. 2006;47:5543-6.

[11] [a] Ooyama Y, Shimada Y, Inoue S, Nagano T, Fujikawa Y, Komaguchi K, et al. New molecular design of donor-π-acceptor dyes for dye-sensitized solar cells: control of molecular orientation and arrangement on TiO_2 surface. New J Chem. 2011;35:111-8; [b] Ooyama Y, Harima Y. Molecular Designs and Syntheses of Organic Dyes for Dye-Sensitized Solar Cells. Eur J Org Chem. 2009:2903-34; [c] Kim D, Lee JK, Kang SO, Ko J. Molecular engineering of organic dyes containing N-aryl carbazole moiety for solar cell. Tetrahedron. 2007;63:1913-22; [d] Li J, Grimsdale AC. Carbazole-based polymers for organic photovoltaic devices. Chem Soc Rev. 2010;39:2399-410; [e] Li J, Dierschke F, Wu J, Grimsdale AC, Muellen K. Poly(2,7-carbazole) and perylene tetracarboxydiimide: a promising donor/acceptor pair for polymer solar cells. J Mater Chem. 2006;16:96-100.

[12] [a] Moon Y, Jeong Y, Kook D, Hong S. Rh(III)-catalyzed direct C-H/C-H cross-coupling of quinones with arenes assisted by a directing group: identification of carbazole quinones as GSKβ inhibitors. Org Biomol Chem. 2015;13:3918-23; [b] Roy J, Pal R, Mal D. Hauser

annulation of furoindolones in the synthesis of carbazole-1,4-quinones and benzo[b]carbazoloquinones. Tetrahedron Lett. 2015;56:6210-3; [c] Do HH, Tran HQ, Ohlendorf L, Ngo TN, Dang TT, Ehlers P, et al. One-Pot Palladium-Catalyzed Synthesis of Benzo[b]carbazolediones. Synlett. 2015;26:2429-33; [d] Bolibrukh K, Khoumeri O, Polovkovych S, Novikov V, Terme T, Vanelle P. Novel Synthesis of 5-Substituted 5H-Benzo[b]carbazole-6,11-diones via Double Buchwald-Hartwig Reaction. Synlett. 2014;25:2765-8.

[13] [a] Clemo GR, Felton DGI. The influence of structure on the ultraviolet absorption spectra of heterocyclic systems. II. Nitrogen analogs of the monobenzofluorenes. J Chem Soc. 1952:1658-67; [b] Bonesi SM, Erra-Balsells R. Electronic spectroscopy of carbazole and N- and C-substituted carbazoles in homogeneous media and in solid matrix. J Lumin. 2001;93:51-74.

[14] [a] Van Duuren BL. Fluorescence spectra of aromatic hydrocarbons and heterocyclic aromatic compounds. Anal Chem. 1960;32:1436-42; [b] Xing Y, Hu B, Yao Q, Lu P, Wang Y. Tandem Synthesis of Benzo[b]carbazoles and Their Photoluminescent Properties. Chem - Eur J. 2013;19:12788-93.

[15] [a] Resch-Genger U, Rurack K. Determination of the photoluminescence quantum yield of dilute dye solutions Pure Appl Chem. 2013;85:2005-26; [b] Lakowicz JR. Principles of Fluorescence Spectroscopy: Springer US, 2007.

[16] Olmsted J, III. Calorimetric determinations of absolute fluorescence quantum yields. J Phys Chem. 1979;83:2581-4.

[17] Frisch M. J. TGW, Schlegel H. B SGE, Robb M. A. CJR, Scalmani G. BV, Mennucci B. PGA. Gaussian 09, Revision C. 01, Wallingford CT: Gaussion: Inc, 2009.

[18] Becke AD. Density-functional thermochemistry. III. The role of exact exchange. J Chem Phys. 1993;98:5648-52.

[19] [a] Adamo C, Barone V. Toward reliable density functional methods without adjustable parameters: the PBE0 model. J Chem Phys. 1999;110:6158-70; [b] Ernzerhof M, Scuseria

GE. Assessment of the Perdew-Burke-Ernzerhof exchange-correlation functional. J Chem Phys. 1999;110:5029-36.

[20] Yanai T, Tew DP, Handy NC. A new hybrid exchange-correlation functional using the Coulomb-attenuating method (CAM-B3LYP). Chem Phys Lett. 2004;393:51-7.

[21] Chai J-D, Head-Gordon M. Long-range corrected hybrid density functionals with damped atom-atom dispersion corrections. Phys Chem Chem Phys. 2008;10:6615-20.

[22] [a] Ditchfield R, Hehre WJ, Pople JA. Self-consistent molecular-orbital methods. IX. Extended Gaussian-type basis for molecular-orbital studies of organic molecules. J Chem Phys. 1971;54:724-8; [b] Hehre WJ, Ditchfield R, Pople JA. Self-consistent molecular orbital methods. XII. Further extensions of Gaussian-type basis sets for use in molecular orbital studies of organic molecules. J Chem Phys. 1972;56:2257-61.

[23] [a] Bremond EAG, Kieffer J, Adamo C. A reliable method for fitting TD-DFT transitions to experimental UV-visible spectra. J Mol Struct: THEOCHEM. 2010;954:52-6; [b] de Lucas NC, Ruis CP, Teixeira RI, Marcal LL, Garden SJ, Correa RJ, et al. Photosensitizing properties of triplet furano and pyrano-1,2-naphthoquinones. J Photochem Photobiol, A. 2013;276:16-30.

[24] Lisboa CS, Santos VG, Vaz BG, de Lucas NC, Eberlin MN, Garden SJ. C-H Functionalization of 1,4-Naphthoquinone by Oxidative Coupling with Anilines in the Presence of a Catalytic Quantity of Copper(II) Acetate. J Org Chem. 2011;76:5264-73.

[25] Liégault B, Lee D, Huestis MP, Stuart DR, Fagnou K. Intramolecular Pd(II)-Catalyzed Oxidative Biaryl Synthesis Under Air: Reaction Development and Scope. J Org Chem. 2008;73:5022-8.

[26] Kraus GA, Man TO. An improved reductive methylation procedure for quinones. Synth Commun. 1986;16:1037-42.

[27] [a] Sridharan V, Martin MA, Menendez JC. Acid-Free Synthesis of Carbazoles and Carbazolequinones by Intramolecular Pd-Catalyzed, Microwave-Assisted Oxidative Biaryl Coupling Reactions - Efficient Syntheses of Murrayafoline A, 2-Methoxy-3-methylcarbazole, and Glycozolidine. Eur J Org Chem. 2009:4614-21; [b] Miguel del Corral JM, Castro MA,

Gordaliza M, Martín ML, Gamito AM, Cuevas C, et al. Synthesis and cytotoxicity of new heterocyclic terpenylnaphthoquinones. Bioorg Med Chem. 2006;14:2816-27.

[28] Kucklaender U, Pitzler H, Kuna K. DNA intercalators, I. Development of 2-hydroxy-benzo[b]carbazole derivatives as cytostatics. Arch Pharm 1994;327:137-42.

[29] Echavarren AM, Tamayo N, De Frutos O, Garcia A. Synthesis of benzo[b]carbazoloquinones by coupling of organostannanes with bromoquinones. Tetrahedron. 1997;53:16835-46.

[30] [a] Schweitzer C, Schmidt R. Physical Mechanisms of Generation and Deactivation of Singlet Oxygen. Chem Rev 2003;103:1685-757; [b] Abdel-Shafi AA, Wilkinson F. Charge Transfer Effects on the Efficiency of Singlet Oxygen Production Following Oxygen Quenching of Excited Singlet and Triplet States of Aromatic Hydrocarbons in Acetonitrile. J Phys Chem A. 2000;104:5747-57; [c] Kikuchi K, Sato C, Watabe M, Ikeda H, Takahashi Y, Miyashi T. New aspects of fluorescence quenching by molecular oxygen. J Am Chem Soc. 1993;115:5180-4.

[31] Jacquemin D, Wathelet V, Perpete EA, Adamo C. Extensive TD-DFT Benchmark: Singlet-Excited States of Organic Molecules. J Chem Theory Comput. 2009;5:2420-35.

[32] [a] Cances E, Mennucci B, Tomasi J. A new integral equation formalism for the polarizable continuum model: theoretical background and applications to isotropic and anisotropic dielectrics. J Chem Phys. 1997;107:3032-41; [b] Mennucci B, Cances E, Tomasi J. Evaluation of Solvent Effects in Isotropic and Anisotropic Dielectrics and in Ionic Solutions with a Unified Integral Equation Method: Theoretical Bases, Computational Implementation, and Numerical Applications. J Phys Chem B. 1997;101:10506-17; [c] Scalmani G, Frisch MJ. Continuous surface charge polarizable continuum models of solvation. I. General formalism. J Chem Phys. 2010;132:114110/1-/15.

[33] Jacquemin D, Perpete EA, Scuseria GE, Ciofini I, Adamo C. TD-DFT Performance for the Visible Absorption Spectra of Organic Dyes: Conventional versus Long-Range Hybrids. J Chem Theory Comput. 2008;4:123-35.

[34] Jacquemin D, Planchat A, Adamo C, Mennucci B. TD-DFT Assessment of Functionals for Optical 0-0 Transitions in Solvated Dyes. J Chem Theory Comput. 2012;8:2359-72.

[35] Jacquemin D, Bahers TL, Adamo C, Ciofini I. What is the "best" atomic charge model to describe through-space charge-transfer excitations? Phys Chem Chem Phys. 2012;14:5383-8.

Figure / scheme Captions

Scheme 1: Preparation of methoxybenzocarbazole derivatives (See Table 1 for substituent details).

Figure 1: Normalized absorption spectra for **5a** in DCM, ACN, Cyh, and MeOH. Concentration variation from 10^{-5} to 10^{-6} mol/L and around 10^{-4} mol/L at expansion.

Figure 2: A) Normalized absorption spectra of **5a** and compounds **5** with a substituent at the R^3 position in cyclohexane. B) Normalized absorption spectra of **5a** and compounds **5** with a substituent at the R^2 position in cyclohexane. Concentration variation from 10^{-5} to 10^{-6} mol/L.

Figure 3: Normalized absorption spectra of **5a** and compounds **5** substituted with methoxy groups in cyclohexane. Concentration variation from 10^{-5} to 10^{-6} mol/L.

Figure 4: Resonance structure representation of a potential extended quinoid type canonical form contribution to the structure of the S_1 excited state of **5** and **6**, and a resonance model representation (**7**) of conjugated electron density delocalization.

Figure 5: Normalized absorption, excitation and emission spectra of **5a** in cyclohexane.

Figure 6: Normalized emission spectra for **5a**: cyclohexane, methanol, dichloromethane, acetonitrile (λ_{exc} = 370 nm).

Figure 7: Part A. Normalized emission spectra of **5a** and derivatives with a substituent at R^3 in cyclohexane (λ_{exc} = 370 nm). Part B. Normalized emission spectra of **5a** and derivatives with a substituent at R^2 in cyclohexane (λ_{exc} = 370 nm).

Figure 8: Normalized emission spectra of **5a** and compounds with methoxy substituent in cyclohexane. For **5a**, **5d**, **5g** and **5f** (λ_{exc} = 370 nm) and for **5e** (λ_{exc} = 365 nm).

Figure 9. Graphical analysis of emission λ_{max} against absorption λ_{max} for **5**.

Figure 10: Fluorescence lifetime determination for **5a** in cyclohexane for an air saturated sample (—) and for a de-oxygenated, argon saturated, sample (· · ·).

Figure 11. Comparison of the calculated (gas phase TD-B3LYP/6-31+G(d)//B3LYP/6-31+G(d), nstates=20) values for $\lambda_{0,0}$ for the $S_0 \rightarrow S_1$ transition with the experimentally observed value of λ_{max} (cyclohexane) for compounds **5**.

Figure 12. TD-B3LYP (nstates=20) calculated UV-vis spectra of compounds **5a** (left) and **6** (right).

Figure 13. Color coded maps of electrostatic potential (ChelpG) for S_0 and S_1 of **5a**, **5f** and **5i** (blue is positive and red is negative).

Figure 14. Cartoon representations of electron density distribution in S_1 as a function of the electronic properties of the substituents R^{1-4}.

Highlights

- Synthesis of novel fluorescent benzocarbazole derivatives by use of C-H functionalization reactions.
- Photophysical characterization: UV-vis, fluorescence emission, quantum yields and lifetimes.
- Study of substituent effects and solvent polarity upon absorption and emission properties.
- (TD)-DFT calculations of the lowest excited singlet states and electron density distribution.
- Characterization of a substituent induced change in the transition dipole moment to S_1.